An Acoustic Emission Activity Detection Method based on Short-Term Waveform Features: Application to Metallic Components under Uniaxial Tensile Test

Fernando Piñal-Moctezuma[a*], Miguel Delgado-Prieto[a] and Luis Romeral-Martínez[a]

[a]Grup de Motion Control and Industrial Applications (MCIA), Departament d'Electrònica, E.S.E.I.A.A.T. Universitat Politècnica de Catalunya, Colom 11, E- 08222 Terrassa, Spain.

Abstract

The Acoustic Emission (AE) phenomenon has been used as a powerful tool with the purpose to either detect, locate or assess damage for a wide range of applications. Derived from its monitoring, one major current challenge on the analysis of the acquired signal is the proper identification and separation of each AE event. Current advanced methods for detecting events are primarily focused on identifying with high accuracy the beginning of the AE wave; however, the detection of the conclusion has been disregarded in the literature. For an automatic continuous detection of events within a data stream, this lack of accuracy for the conclusion of the events generates errors in two critical aspects. In one hand, it deteriorates the accuracy of the measurement of the events duration, truncating the span of the event, which is undesirable in evaluation applications; and in the other hand, it causes false detections. In this work, an accurate and computationally efficient AE activity detector is presented, using a framework inspired by the area of speech processing, and which provides the required indicators to accurately detect the onset and the end of an AE event. This is achieved by means of a threshold approach that instead of directly operates with the transduced voltage signal it does so over the Short-Term Energy and the Short-Term Zero-Crossing Rate measures of the signal. The STE-ZCR method is developed for an application related to the continuous monitoring of a single AE channel derived from the characterization of metallic components by means of a uniaxial tensile test. Additionally, two experimental test-benches are implemented with the aim to quantify the accuracy and the quality of event detection of the presented method. Finally, the obtained results are compared with four different techniques, representing the current state of the art related to AE activity detection.

Keywords

Acoustic Emission, Short-time analysis, Onset detection, Endpoint detection, Detection algorithms, Performance analysis.

1. Introduction

Due to high demanding specifications on safety and reliability demanded by the transportation sector, the design and manufacturing of metallic components and particularly for this end, the accurate mechanical characterization of these materials, represents a critical aspect in which a great deal of technical and scientific efforts have become essential [1,2]. In this regard, one of the most used methods is the tensile test [3,4], in which some important mechanical properties as the Young's modulus, the Poisson's ratio and the yield strength point are measured. One of the outcomes of the assay is the strain experienced by the specimen, typically measured by means of strain gauges and extensometers. Nowadays, in order to complement the accuracy delivered by these devices, efforts have been made in order to implement additional instrumentation to the test. Such is the case of video extensometer systems, allowing a forensic analysis based on image processing; nevertheless this approach presents two main restrictions, first, the frame digitization period which usually is in the range of unit of milliseconds, and second, the limitation to the surface monitoring which implies a significant loss of information about the internal material dislocations [5]. An alternative mechanical

descriptor considered to be added to the test [6], is the analysis of the Acoustic Emission (AE) phenomenon. Which is the manifestation of transient elastic waves in a material, produced by irreversible changes in its crystalline structure. This has been exploited as a potent mean to assist in the detection, location or evaluation of damage.

For the AE as an assessing damage tool, the processing chain is usually composed by the transduction and acquisition of the phenomenon and in the separation and analysis of each captured AE wave. Particularly, for the separation stage of AE events, due to the inherent features of the phenomenon, the resulting waveform from the acquired signal implies a very challenging task in which to be able to perform a proper identification and separation of each AE event; this mainly caused by exhibiting a highly varying background noise, a large difference of amplitudes between events, and a randomness on the incidence and lifespan of these AE events.

Traditionally, the detection work is carried out by the comparison with the acquired electrical signal against a predefined voltage threshold level, in which whenever the electrical signal rises above of this fixed level, it is said that an AE event has been detected. This method, implemented in the early days of using AE as a damage detection tool, emerged due to the then-contemporary lack of available digital hardware capable to process the payload from the large data stream required for a proper digital treatment of the practically baseband signal [7]. Nowadays, after the advent of digital platforms and given its relative efficiency and ease of implementation, nearly all the established standards for AE [8,9], as well as the commercially available instrumentation and in consequence the majority of the fieldwork, have inherited this voltage thresholding design paradigm as the default method for detecting AE activity. Nevertheless, this method does not directly deal with the abovementioned particularities of the acquired waveform, yielding to inaccuracies on the onset and endpoint determinations related to the AE events; and as in consequence, eventually causing a degradation of the information obtained from the process of assessing.

Efforts have been made in order to overcome the aforementioned limitations of the classical thresholding approach, where methodologically, most of the developed methods carry out a transformation of the raw electrical signal into a Characteristic Function (CF) with the aim of emphasizing the presence of AE events, thus enabling a more efficient detection work. Based on non-parametric signal processing methods, the Time-Frequency distribution analysis represents a more accurate tool for detecting the temporal onset of the AE waves; currently most of the efforts are focused on the use of the Wavelet Transform (WT) [10–14], due to improving the resolution of the energy localization of the AE event in the Time-Frequency plane and in consequence having a better accuracy for the onset determination of the AE wave. Most of these advanced techniques find their inspiration into the Geophysics discipline due to the similar production between phenomena, such is the case of the Short-Term Average to Long-Term Average ratio (STA/LTA) [15], developed for determining earthquake events while maintaining a low count of false-positive alarms. The most revised technique in the AE area, is the Akaike Information Criterion (AIC) [16], that models the time series data at the beginning of the AE raw signal under a low order autoregressive scheme, with the aim of achieving an estimation of two locally stationary parametric components of the framed original signal, noise and AE activity, hence allowing the identification of the AE onset.

Despite of advanced methods clearly represent superior alternatives to the classic thresholding technique, traditionally they have evolved in light of applications for locating AE sources, where a highly accurate onset detection is critical, so consequently, issues related to the endpoint determination have been disregarded. Methodologically, this imply that instead of considering some intrinsic feature related the phenomenon, all the AE activity detection methods only make use of the combination of a threshold level along with a fixed timer in order to determine the conclusion of the AE event. Nevertheless, due to the stochastic manifestation of said events, this methodology leads to inaccuracies on the measurement of the endpoint determination, and

in consequence, directly affecting to the quality of detection of all methods, i.e., the amount of properly detected AE events on a survey [17]; being a critical aspect for damage assessing applications.

A last matter to considering is that due to the high data rates required to process the AE phenomenon, these advanced methods are computationally expensive, so usually they are implemented under an offline framework, i.e., first capturing the data from the survey to later separating the AE events. Although some efforts have been made in order to implement hardware architectures that can operate under an online approach [18–20], there are still required strategies that can lead to faster and efficient implementations, this particularly necessary for long surveys.

Evidently, Acoustic Emission is not the only discipline related to the Signal Detection Theory (SDT). Particularly in the speech processing discipline, SDT finds its application on the Voice Activity Detection (VAD) stage [21,22]; where a randomly present speech activity from a highly noisy digitized signal aims to be extracted in order to reduce the payload from the subsequent stages given a particular application, e.g., voice telecommunications, artificial intelligence, hearing aids among others. One of the best-established automatic VAD for the speech processing area is the technique developed by Rabiner and Sambur [23]. This parameter-based VAD was originally designed with the objective to accurately detect the beginning and the end of an utterance, while preserving an efficient and straightforward processing scheme as well as being robust against varying background noise. This was achieved with the use of two indicators of the signal: the Zero-Crossing Rate and the Short-Term Energy. Additionally, the algorithm was intrinsically capable of suitably executing in any realistic acoustic environment in which the Signal-to-Noise Ratio (SNR) was in the order of 30dB. Despite of the dissimilar origins between Acoustic Emission and Speech phenomena, and consequently the technical requirements in order to be processed, e.g., instrumentation, bandwidth of 8kHz vs. 1MHz, etc.; behaviors on their waveforms share similar characteristics, such is the case of a high variance on the occurrence of activity, rapid varying background noise and significant dynamic range.

In this work, an AE activity detector inspired by the voice activity detector developed by Rabiner and Sambur [23] is presented. The AE detector is revised for an application related to the recording of a single channel from a continuous monitoring, derived of the characterization of a metallic component by means of an axial tensile test, where the AE waves derived from this assay typically exhibit large amplitude differences between events, stochastic occurrence and duration, and highly varying mechanical background noise due to cumulative reflections.

In order to evaluate the performance of the presented STE-ZCR method, two experimental setups are arranged: a) a collection of Hsu-Nielsen sources with aim to quantifying the accuracy of the onset and endpoint determinations as well as for assessing the robustness of the method with regard to induced background noise. b) The continuous detection of AE events from an AE data stream obtained from a standardized tensile test in order to quantify the quality of detection of this method. Additionally, with the aim to establishing a common benchmark of comparison with some of the advanced detection techniques currently available in the literature, the results of the presented method are compared with: a) A classical threshold technique enhanced by means of the Instantaneous Amplitude [24], b) A typical STA/LTA detector [25], c) A two-step AIC picker [26], d) An a CWT-Otsu detector over a binary image mapping [14] which alike c) uses a modified Allen's Formula as CF for the threshold-based early detection.

Contribution of this work is to providing an automatic AE event detector for a continuous data stream, which excels the detection capabilities, i.e., the onset and endpoint measures, as well as the detection quality of events with regard to the existing methods present in current literature. Novelties of this work include the use of the Short-time analysis, which offers an accurate, noise resilient and computationally efficient framework with aim to detecting AE events. In addition, and instead of using the traditional combination of a threshold level

and a fixed timer, the implementation of an indicator extracted from the waveform of the signal with the aim to determining the conclusion of an AE event

This paper is organized as follows: In Section 2 the proposed STE-ZCR detection method is introduced. Section 3 describes the two experimental setups with the aim of benchmarking the method and comparing its performance with the current advanced methods from literature. In Section 4, results are presented and discussed. Finally, in Section 5 conclusions are provided.

2. Methodology: AE Activity Detector

The idea behind of the Short-Time or Short-Term Analysis (ST-ANLYS) relies on the stationarity of time series, with the aim to creating a new sequence that can represent some varying feature of the original signal. This can be achieved based on the fact that some signals such is the case of an AE signal, intrinsically will not show stationary behavior, that is, during their durations there will not be clear tendency of repeatability, e.g., statistical mean and covariance. However, when the signal is enough and equally time-frame segmented, it will show a relative slow variation for some property between segments, so these time segments, usually known as analysis frames, will relate the analysis of the signal regarding a fixed size time window.

An activity detector exploits this artificial induced stationarity by identifying the relatively higher energy and lesser number of zero crossings associated to a phenomenon under development. Despite of the inherent uncertainties induced by the short-term analysis, it has proven to be an efficient tool with the aim of identifying the regions of activity of a signal.

For this work, the STE-ZCR method (see Fig. 1), firstly is composed of the generation of two characteristic functions derived from the short-term analysis of the Energy and the Zero Crossing Rate regarding to the acquired AE signal; and secondly, by the detection of AE events performed by a dedicated algorithm taking as inputs these pair of characteristic functions.

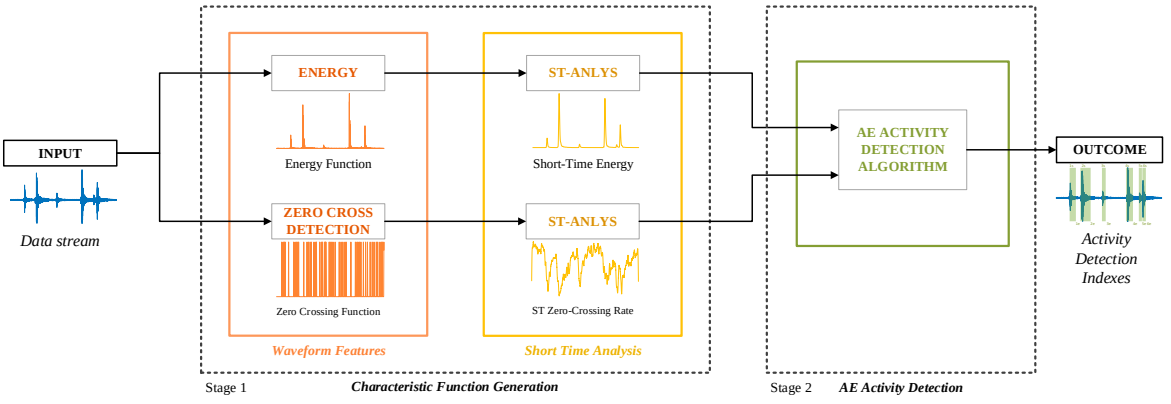

Fig. 1. Block diagram for the STE-ZCR method, composed by two main stages: 1) Production of two CF by means of the ST-ANLYS framework, and the 2) Activity detection algorithm aimed to searching for the onset and endpoint by means of the STE and the ZCR respectively. For each detected AE event, outcome of the method consists of a pair of indexes that mark the temporal start and end sampling points with regard to the data stream.

2.1 Stage 1. Characteristic Functions Generation: Short Time Analysis Framework

2.1.1 Short-Time Energy

As is known, the energy E of a discrete-time signal of length L from a point of view of signal processing can be expressed as $\sum_{m=0}^{L}|x(m)|^2$. For this framework, the short-time energy of the signal is defined as:

$$E_{\hat{n}} = \sum_{m=\hat{n}-N+1}^{\hat{n}} |x(m)|^2 \, w(\hat{n}-m) \tag{1}$$

where $w(\hat{n}-m)$ is a window function of N width, centered at sample $\hat{n}$, and where $\hat{n}$ in turn indicates the overlapping factor between windows through the relation $\hat{n} = kT$, with $k = 0, 1, ...$, and $T < N \leq L$.

For this AE activity detection application, and since values of $E_{\hat{n}}$ for an AE wave are considerably greater than noise floor energy, the association of $E_{\hat{n}}$ lies in provide a measure for separating the presence of AE waves from idle activity on the studied sequence. It is important to note that under this approach, there are three different parameters to configure for the short time analysis of the energy:

a) Window function. Since the characteristic function derived from the short-time analysis will strongly depend on the choice of the selected window, and since the objective is to highlight a feature of interest of the evaluated signal, windows must meet some requirements e.g., smoothness, non-negative terms, compact support, square integrable resultant products. For activity detection related applications, by properly concentrate the energy of the signal in the time domain and meet the aforementioned requirements, typically used windows belongs to the raised cosine families e.g. Hamming, Hanning, Blackman, etc.

b) Window length. Ideal response of the characteristic function is to depicting the feature of interest at a rate time comparable of the original signal. Short-term analysis will inherently portray uncertainties on the temporal relocations of the analyzed feature due to a mistaken selection of the length, i.e., small lengths will not reveal signal stationarity, medium lengths will lose rapid transients, and large lengths will suppress the dynamic of the signal. Consequently, selection of the length of the window will entirely rely on the related application, making it necessary to considering the tradeoffs on the responsiveness of the analysis. For the case of the AE phenomenon, despite that duration of the events randomly behaves from nanoseconds up to hundreds of milliseconds, representative AE lifespans are in the order of the microseconds. Thus, for AE related applications, windows of duration in tens of microseconds should be a balanced selection that meet the abovementioned criteria. Nonetheless, in order to characterize the expected AE waves, it is highly desirable to perform a prior calibration based on the properties of the studied material by means of artificial Hsu-Nielsen sources.

c) Window overlapping factor. To reveal stationarity, short-term analysis requires sliding the configured window over the signal of interest. Although, with the objective of reducing the computation load, the overlapping of data frames is typically implemented, in the case of applications where temporal accuracy is critical when revealing stationarity, as is the case of the AE, it is highly recommended to avoid overlapping, i.e., by performing the direct convolution of the window function and the AE signal.

2.1.2 Short-Time Zero Crossing Rate

The zero-crossing point for an alternating electrical signal is the instantaneous time value when voltage equals to zero. Since the point of view of the discrete-time signal processing, a zero-crossing point occurs where two

adjacent sampling points on the sequence have different mathematical signs, i.e., showing opposite polarities. This feature, represents a straightforward approximation for measuring the noisiness, as well as to coarsely infer the dominant frequency and spectral centroids of signals; and it has been extensively used for different disciplines with the aim to discerning between activity conditions [27–29].

In the case of AE signals, once an AE wave reaches the sensor, pressure will be exerted over the surface of this, producing in turn a rapid rise on the transduced amplitude levels; and consequently, while the AE wave exists, decreasing the speed of the alternation of the electrical signal over the zero-volt axis. With the objective to identify the presence of AE events, this trend change of the signal can be exploited by correlating the high-speed zero crossing rate with the absence of AE waves, and the low-speed zero crossings regarding to the existence of AE events.

For an AE signal, in this work, the rate count of zero-crossings per frame is described as:

$$Z_{\hat{n}} = \frac{1}{2N} \sum_{m=\hat{n}-N+1}^{\hat{n}} |sgn(x[m]) - sgn(x[m-1])|\, w(\hat{n}-m) \tag{2}$$

where $w(\hat{n}-m)$ is the chosen window function, N is the length of said window, and also indicating the overlapping factor between windows through the relation $\hat{n} = kT$, with $k = 0, 1, ...$, and $T < N \leq L$. Finally, sgn denotes the signum operator defined as:

$$sgn(x[n]) = \begin{cases} 1, & x[n] \geq 0 \\ -1, & x[n] < 0 \end{cases} \tag{3}$$

Still, is possible to express the ZCR normalized for an interval of M-samples, whence ZCR becomes:

$$Z_M = MZ_{\hat{n}} \tag{4}$$

where for an interval of τ seconds and sampling frequency F_s of the acquired AE data, the number of samples of M are:

$$M = \tau F_s \tag{5}$$

Finally, as in the case of the STE, the ZCR characteristic function is also based on the short-time analysis; therefore, in order to obtain a proper description, it is also necessary to make the same considerations about type, length and overlapping of the window with regard to the properties of the studied material. Furthermore, it is highly advisable for a STE-ZCR framework to use identical windows for the generation of both functions.

2.2 Stage 2. AE detection algorithm

Once that both characteristic functions, STE and ZCR are obtained, the second stage of the STE-ZCR method consists of finding the pairs onset-endpoint regarding to the AE events on the signal. For this, based on the fact where the waveform derived from an AE event will exhibit higher energy and lesser ZCR count, it is possible to set up the basis to implement an algorithm that can detect AE events on a straightforward but yet efficient scheme (see Fig. 2).

The algorithm makes use of two different fixed threshold values for its operation, the *Identification Threshold Upper* (ITU) that works on the STE signal in order to detect new AE events and the *Identification Zero Crossing Threshold* (IZCT) that works on the ZCR with the aim to determining the endpoint for a detected

AE event. Thus, a previous characterization of the instrumentation with regard to the surveyed material is highly recommended to characterize the background noise level and the amplitude of the electrical waveform of the monitored AE channel, in order to carry out a proper calibration of said threshold parameters. In addition to the characteristic functions generated by means of the short-term analysis, the algorithm makes use of the derivative of the STE with the aim to refine the onset determination of the AE event. Finally, with the purpose to enhance the quality detection, a basic adaptive threshold scheme is implemented by continuously taking measurements of background noise and adjusting the threshold levels between search iterations.

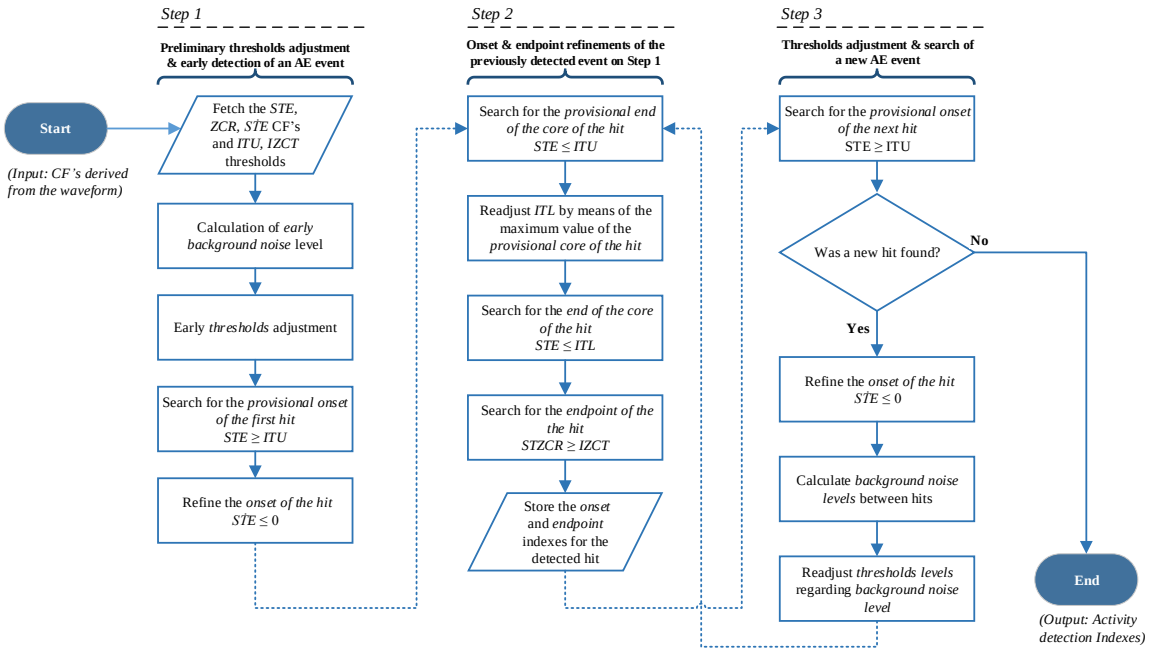

Fig. 2. Flowchart for the activity detection algorithm composed of three main steps: 1) Preliminary calculation of background noise for an idle state of the signal, 2) Search job for the onset and endpoint of a hit, 3) Threshold level adaptation regarding to the updated background noise. Reader is also referred to Fig. 3 for a visual instance of the characteristic functions and threshold levels used by the algorithm.

The search work begins by estimating the *early background noise level* related to the STE, for a small segment of the sequence belonging to the beginning, since it is assumed that there is not exists any AE event yet. This noise estimation is achieved by means of the sum of the arithmetic mean $\bar{x}_{STE}$ and the α-weighted factor for the standard deviation σ_{STE} of the STE signal, where this α factor can be estimated along with the previous calibration for the thresholds, if a heavy background noise is expected the value for this weighting value must be incremented. In order to perform the first threshold adaptation, the *early background noise level* is added to the preset *Identification Threshold Upper* (*ITU*), expressed in levels of energy (v^2.s) $ITU_{adjust} = ITU + (\bar{x}_{STE} + \alpha * \sigma_{STE})$.

For the calculation of the ZCR *early background noise level*, same calculations performed in the STE case, are carried out over the same segment length belonging to the ZCR. Thus, the resulting *adjusted Identification Zero Crossing Threshold* will be: $IZCRT_{adjust} = IZCRT + (\bar{x}_{ZCR} + \alpha * \sigma_{ZCR})$, expressed in form of the normalized ZCR, for a length window of *M* samples ($\widehat{ZCR}$). Additionally, for this parameter, with the purpose to use a simpler threshold presetting, it is also possible to process the *IZCT* threshold value like a percentage of the computed *early background noise level*. Next step consists of finding the first sample $n_{Prov-onset}$ in the *STE* sequence where: $STE[n] \geq ITU_{adjust}$; this $STE[n_{onset}]$ sample will be the *provisional onset hit*.

The last task for this first stage comprises of the refinement of the onset detection of the hit by means of the first derivative of the STE sequence, namely $\dot{STE}$. The purpose on the use of this signal is to take advantage of the sensitivity to the energetic change that the STE provides, by finding the first occurrence of the energetic variation of the captured AE phenomenon. Thus, it is possible to assume that in this sample the arrival of p-waves is manifested. For this, it is carried out a backward search from the corresponding $\dot{STE}$ sample of the *provisional onset hit* sample until finding the $n_{true-Onset}$ sample where $\dot{STE}[n_{true-onset}] \leq 0$. This sample is indexed as the *true onset hit detection*, and it will be the first outcome of the search job.

The first task for the second stage in the algorithm consists of finding the *core of the hit*. Since in this region most of the AE wave energy is concentrated, it is necessary to delimit it accurately with the aim to aiding to find the duration of the hit. For this step, the first subtask requires to finding the *provisional end of the core of the hit* $n_{provEoC}$, this can be picked up readily by locating the first sample from the *provisional onset hit* sample where $STE[n] < ITU$.

Next, for the search work of the *end of the core of the hit*, it is required to find the maximum value $STE_{max-core}$ regarding to the provisional core of the hit, i.e., the range between *STE*[*provisional onset hit*] and *STE*[*provisional end of the core of the hit*], to then readjust the *Identification Lower Threshold* (*ITL*) expressed in levels of energy (v^2.s). With the aim to achieving an accurate readjust for this threshold level, it is necessary to establishing a model that aids to properly determine the behavior of the amplitude distribution level for the processed AE events.

Mathematically, the realization of the AE phenomenon is conceived as a non-stationary stochastic signal [30,31]. Still, after being transduced by a sensor, the resulting AE waveforms are traditionally treated as radio pulses in exponential decaying. Accordingly, a widely used waveform model [32–38], considers to the electrical AE signals as underdamped sinusoidal functions of the form:

$$AE_{signal}(t) = \begin{cases} A\,exp\left(\frac{-t-T}{\gamma}\right) sin\, 2\pi v_0 (t-T)\,, & t \geq T \\ 0, & t < T \end{cases} \tag{6}$$

where A is the amplitude and T is the arrival time of the AE wave; γ and v_0 the decay constant and the resonant frequencies belonging to the sensor.

Thus, it is possible to modelling the envelope $e(t)$ regarding to the AE wave [39,40], after reaching a maximum value K at time T_e, as an exponential decay function:

$$e(t) = Ke^{-v_0 t}, \qquad t \geq T_e \tag{7}$$

being v_0 the decay constant belonging to sensor.

It is evident that this simple model can be further enhanced, still, for the application of this work, it is only necessary to identify that the STE corresponding to an AE wave behaves as an impulse response function regarding to a linear-time-invariant dynamical system of first order. As is well known, the time constant τ, which characterizes the response of this system and its bandwidth for a system like in Eq. 7, it is located at the instant of time t_τ where $e(t_\tau)$ equals to 36.8% of its maximum value. Therefore, taking advantage of this fact, it is possible to assume that the core of an AE wave will expire when the STE characteristic function, equals to the 36.8% of its maximum reached value. Hence, the value for the *Identification Lower Threshold* will be adjusted to $ITL = 0.368 STE_{max-core}$ with the aim to then perform a forward search from $STE[n_{max-core}]$ until find the n_τ sample where $STE[n] \leq ITL$.

This n_τ sample will be the *end of the core of the hit*. While it is true that after the *end of the core of the hit* most of the energy of the AE wave is nearly vanished, the region between this *STE* endpoint detection and the one that will be determined through the ZCR, still will comprise a relevant content of energy. Thus, the joint use of these pair of characteristic functions will provide a more robust and precise approach for determining the end of the lifespan of the AE wave. For this, a simple search forward over the ZCR sequence will be performed from the *end of the core of the hit* n_τ sample, until finding the $n_{endpoint}$ sample where the ZCR sequence be greater than the *Identification Zero Crossing Threshold*, i.e., $ZCR[n] \geq IZCT_{adjust}$. This sample will be indexed as the *true endpoint of the hit*. With these two indexes, *true onset hit detection* and *true endpoint of the hit* as outcome of the algorithm, it concludes the work for the second stage of the algorithm and the third and last stage of this can be executed, by searching a new AE event over the STE sequence, and using the last adjusted value of the *Identification Threshold Upper* from the *true endpoint of the hit* sample. Once detected, a refinement of the onset task by means of the STE derivative will be performed.

Next, an update of noise levels regarding to their corresponding characteristic functions will be performed from the last *true endpoint of the hit* to the new *true onset hit detection*, to then readjusting of the *Identification Threshold Upper* and *Identification Zero Crossing Threshold* values. Still, with the purpose of avoid the overlapping of AE events, if a new event were detected before the *true endpoint of the hit* sample by means of the *Zero Crossing Rate* function, the *true endpoint of the hit* must be readjusted to one sample before of the *true onset hit detection*. Finally, the second stage of the algorithm will be performed again and the described iteration is repeated until all events of the sequence under analysis are detected.

In Fig. 3, it is shown the operative stages related to the STE-ZCR AE detection technique, using two different AE events and their corresponding durations determined by the AE activity detector indicated by green shaded areas (Fig. 3a).

For the onset detection work, in Fig. 3b it can be observed the Short-time Energy characteristic function (blue-steel area under the curve), the preset threshold level (horizontal dotted black line), the signal segment for the early background noise calculation (yellow shaded area), the first adjusted Identification Threshold Upper (horizontal dotted yellow line) and the sample of activation for the first AE event (first vertical solid yellow line), the signal segment for the second background noise calculation (lilac shaded area), the second adjusted Identification Threshold Upper (horizontal dotted lilac line), the sample of activation for the second AE event (vertical solid lilac line), the Identification Lower Threshold (horizontal dotted white line) for each AE event, as well as the segment for the end of the core search job (red shaded areas). Finally, as outcome for this stage it is shown the core of the hit (gray shaded areas).

For the refinement work related to the onset detection, in Fig. 3c it is depicted the backward search job carried out over the derivative function of the STE (blue solid curve), which starts from the beginning of core of the hit (vertical dash-dotted black line) until finding a value equal or lesser than zero (vertical solid green lines).

Finally, in Fig. 3d it is represented the endpoint determination work by means of the Short-time Zero Crossing Rate characteristic function (blue solid curve), it can also be observed the segment for the early background noise calculation (yellow shaded area), the samples of activation *end of the core of the hit* (vertical dotted red lines), the first adjusted Identification Zero Crossing Threshold (horizontal dotted yellow line), the signal segment for the second background noise calculation (lilac shaded area), the second adjusted Identification Zero Crossing Threshold (horizontal dotted lilac line), as well as the endpoint determination samples (vertical solid green lines) as outcome for this final stage of the search algorithm.

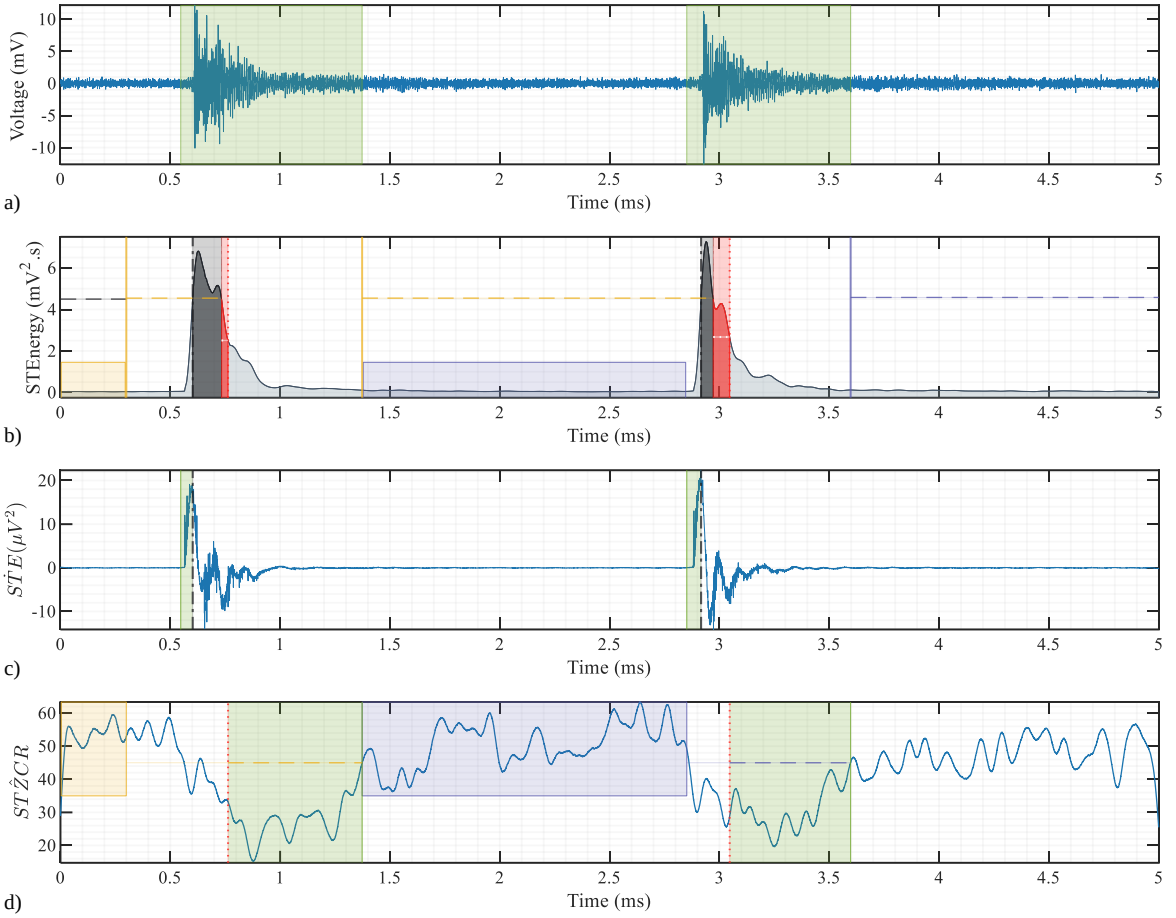

Fig. 3. Depiction of the STE-ZCR detection method for a 5ms data-frame containing two AE events. a) AE events and their respective automatic duration determinations (green areas) as final outcome. b) Onset detection work by means of the STE characteristic function. c) Onset refinement with the STE derivative. e) Endpoint determination using the ZCR characteristic function.

3. Experimental procedures

Following the experimental procedures presented in the literature, two experimental scenarios were arranged with the aim to quantifying the competency of the proposed STE-ZCR method in front of a comparative common framework with regard to some of the most significant methods for detection of AE events from literature.

First experimental scenario is prepared to quantifying the precision of the measures regarding to the onset, endpoint and lifespan determinations. For this, a collection of one-hundred different AE waves derived from a standardized Hsu-Nielsen test is processed and their corresponding detection absolute errors are calculated. Then, with the purpose of evaluating the operating robustness in front of noise, each AE synthetic wave of the dataset is tainted with three different levels of Additive White Gaussian Noise (AWGN), and their corresponding detection absolute errors once more are calculated. Additionally, in order to evaluate the computing throughput of the presented method, the processing time of each analyzed AE event is measured.

The second test-bench involves to measuring the quality of detection by means of the accuracy, precision, sensitivity, f1-score, false-discovery rate and false-negative rate statistical indicators. For this, a data frame derived from a tensile test of a metallic component containing an ample variety in duration, amplitude and incidence of AE waves is processed, and the amount of properly detected AE events is totaled. The required processing time with regard to the data frame is also calculated, as well as the absolute errors of the onset, endpoint and lifespan detections of the corresponding true-positive events.

For both experimental scenarios, one sensor (Physical Acoustics WSα, 100-1000 kHz) was attached to the surface of each corresponding metallic component, using a silicon-based couplant agent. The resulting electrical signals were amplified by a Mistras preamplifier 2/4/6 with a bandwidth of 10-2500 kHz and using a gain of 20dB. The amplified electrical signals, were recorded under a free-running sampling scheme, using a CSE4444 digitizer of the GaGe manufacturer, with a sampling frequency of 5MHz for the Hsu-Nielsen data and 10MHz for the tensile test data, for both scenarios a resolution of 16-bit depth is used. All the raw signals are band-pass filtered in a frequency band of 10-2200 kHz, by means of a FIR equiripple implementation. Preliminary to performing the corresponding test-benches, the onset and endpoint times of each AE-wave that will be processed, are manually picked supported by means of time-voltage plots as well as by a time-frequency distribution of high resolution [41].

Test benches as well as the considered methods are implemented using software scripts executed by MATLAB® R2018a in a PC with a CPU Intel Core i7-6800k (3.4GHz) and 64GB of DDR-2400 RAM.

For the state of the art methods used in the experimental scenarios, the most fitting calibration parameters in regard to the test-bench are done following the recommendations of related literature [26,42–46] as well as the current standards [8,9,47–51].

3.1 Hsu-Nielsen data test-bench

For the Pencil-Lead Breakage (PLB) test-bench, and for each of the one-hundred realizations, a graphite lead of ⌀ 0.5mm, 2.5mm tip-length and applying a contact angle to the surface of the metal sheet specimen of 60° is used. In addition, a distance of 12cm between source and sensor is preserved (see Fig. 4).

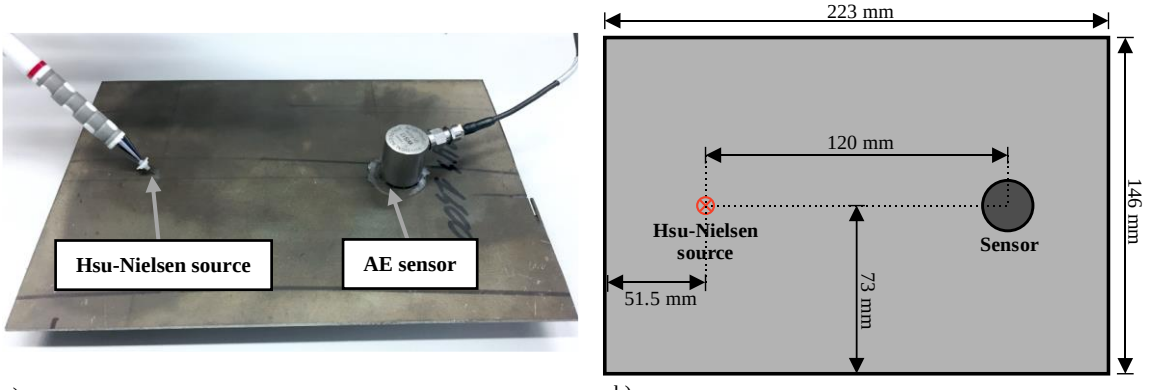

Fig. 4. Setup for the standardized Hsu-Nielsen test-bench over a Press-Hardening 1500 steel plate specimen. (a) Photograph of the AE sensor, the guide-ring tube used to generate the artificial sources and the steel plate (stood over a foam base). (b) Schematic diagram indicating the dimensions of the specimen and the locations of the source and sensor.

For a frequency range of up to 1MHz, the average phase velocity for the extensional mode is of 5194m/s and for the group velocity case is about of 4471m/s. In Fig. 5, it is shown the characterization of the used sheet specimen by means of its dispersion relation of the fundamental Lamb wave modes (obtained using the Wavescope software [52]). With this information, and considering the operative frequency of the used sensor, the source-sensor layout shown in Fig. 4 and assuming an ideal isotropy in the material, it is possible to neglect the effect of the change of velocity for this experiment.

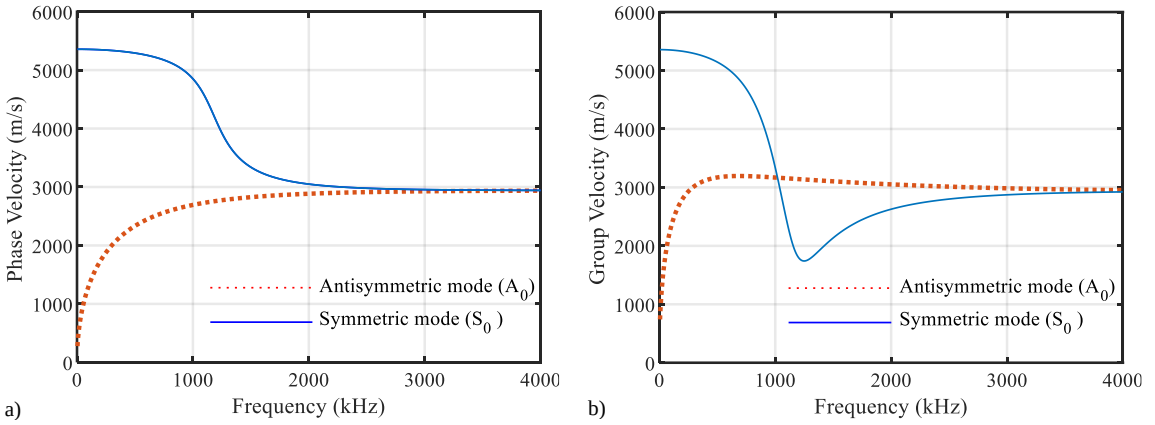

Fig. 5. Fundamental dispersion curves of the Press-Hardening 1500 steel sheet with a thickness of 2mm, Young's modulus of 211GPa, density of 7850kg/m^3, Poisson's ratio of 0.3 and shear modulus of 83GPa. (a) Phase velocities. (b) Group velocities.

For repeatability purposes, each synthetic AE wave is edited so its peak value is centered on 5ms and the signal be extended during 40ms more, as a result, each AE wave from the data set collection will exhibit an average lifespan of 20.86 ± 1.16ms. A typical waveform obtained from this process is shown on in Fig. 6.

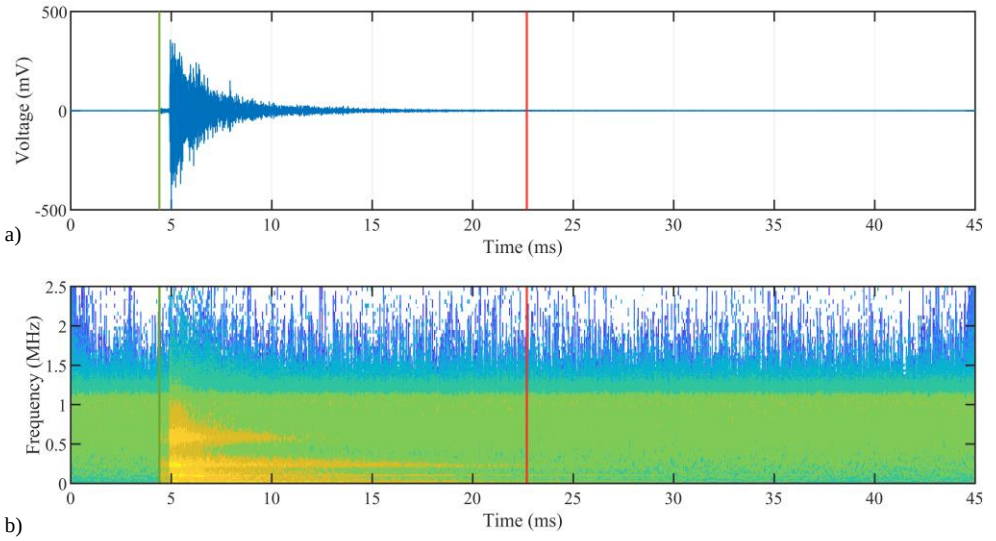

Fig. 6. Typical AE waveform event analyzed in the synthetic data test-bench. (a) Time-Voltage representation. (b) Synchrosqueezed wavelet transform, by means of an analytic Morlet wavelet, and used to assist in the manual determination of the beginning and conclusion related to AE events. Green and red lines in figures indicate the manually picked onset and endpoint locations respectively.

3.1.1 Operational robustness in front of background noise

Second objective for this test-bench consists of evaluating the operational robustness of the STE-ZCR method in front of background noise. For this, since each AE wave from the data set collection exhibits an average Signal-to-Noise Ratio (SNR) of 27.1 ± 1.15dB, their corresponding SNR is decreased by means of AWG noise in three different rounds of analysis of 20, 15 and 10 dB respectively (see Fig 7). Then, the relative errors for the onset, endpoint and lifespans are newly calculated for each round, as well as the consumed processing times.

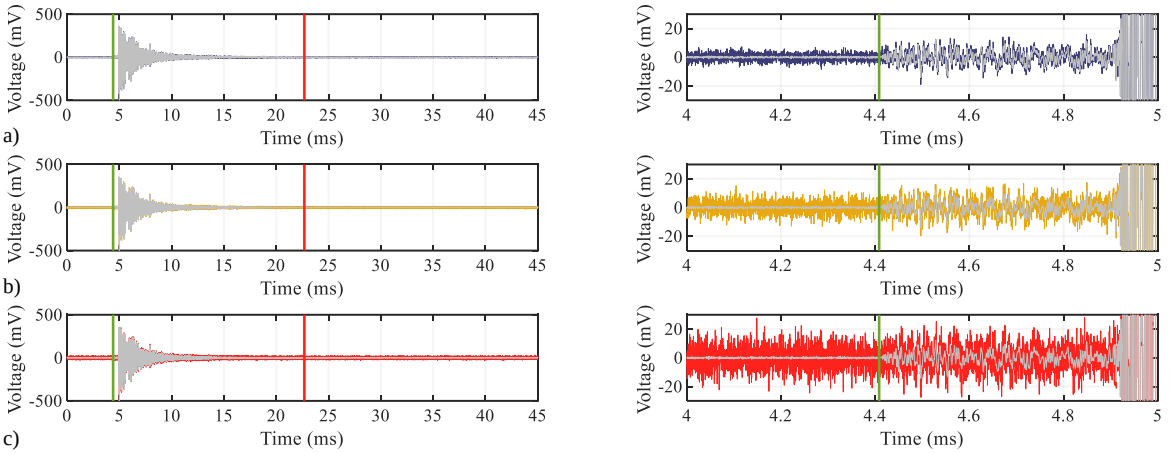

Fig. 7. Example of an AE wave used for the evaluation of operational robustness against noise, and onset and endpoint locations (green and red lines respectively). In the test, a synthetic AE signal (gray) is tainted by AWGN in order to obtain three different signals with levels of SNR of: (a) 20dB (lilac), (b) 15dB (yellow), (c) 10dB (red). Images of the right column show a 1ms zoom of the corresponding data frame for the wave onset.

3.2 Uniaxial tensile test

The objective for the second test-bench is to quantify the quality of event detection by means of statistical indicators in front of field data. For this, a tensile test of a metallic component is carried out (see Fig. 8).

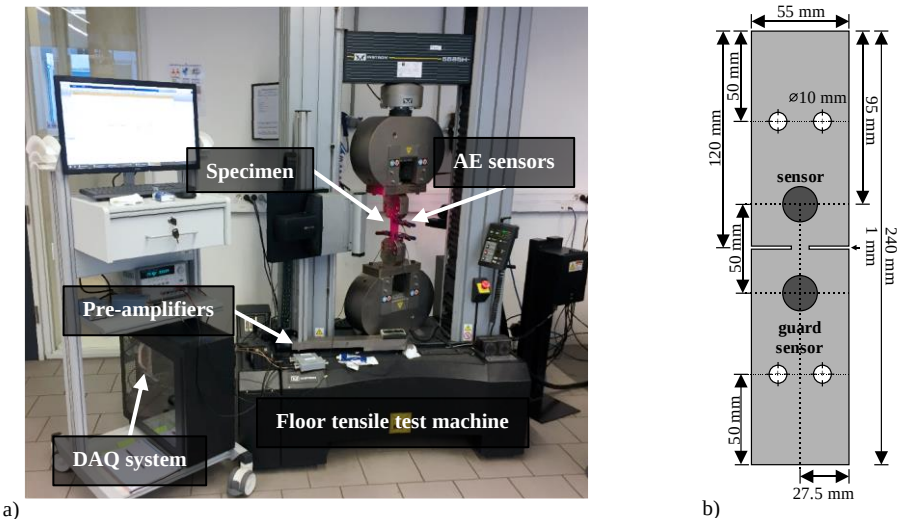

Fig. 8. Setup for the tensile test-bench over a Ferrite-Pearlite annealing steel sheet specimen (load rate of 1mm/min). (a) Photograph of the used instrumentation and test machine. (b) Schematic diagram indicating the dimensions of the metallic specimen and the locations of the sensors.

Although a pair of identical sensors were attached during the assay, for this test-bench, only the signal of the main sensor will be analyzed. For this experimental scenario, by considering the operative frequencies range of the sensor and its location over the specimen (see Fig 8.), and if it is assumed an ideal isotropy in the material, for the characteristic average extensional mode wave velocities of ~5104m/s for the phase and ~4348m/s for the group (see Fig. 9), it is possible to neglect the effect of the change of velocity for this experiment.

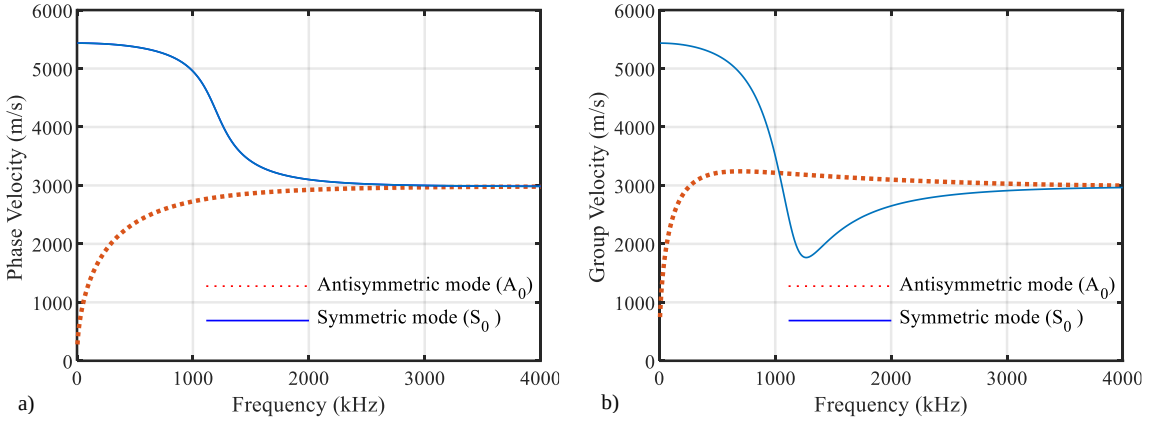

Fig. 9. Fundamental dispersion curves of the Ferrite-Pearlite annealing steel sheet with a thickness of 2mm used in the experimental scenario, with Young's modulus of 205GPa, density of 7850kg/m^3, Poisson's ratio of 0.3 and shear modulus of 83GPa. a) Phase velocities. b) Group velocities.

The AE signal produced by the tensile test was collected; and for the experimental scenario a frame length of 500ms containing 380-AE events is used as the input for each detection method (see Fig. 10). For each AE event, the onset and endpoint locations are manually picked supported by the frame waveform and its corresponding time-frequency distribution.

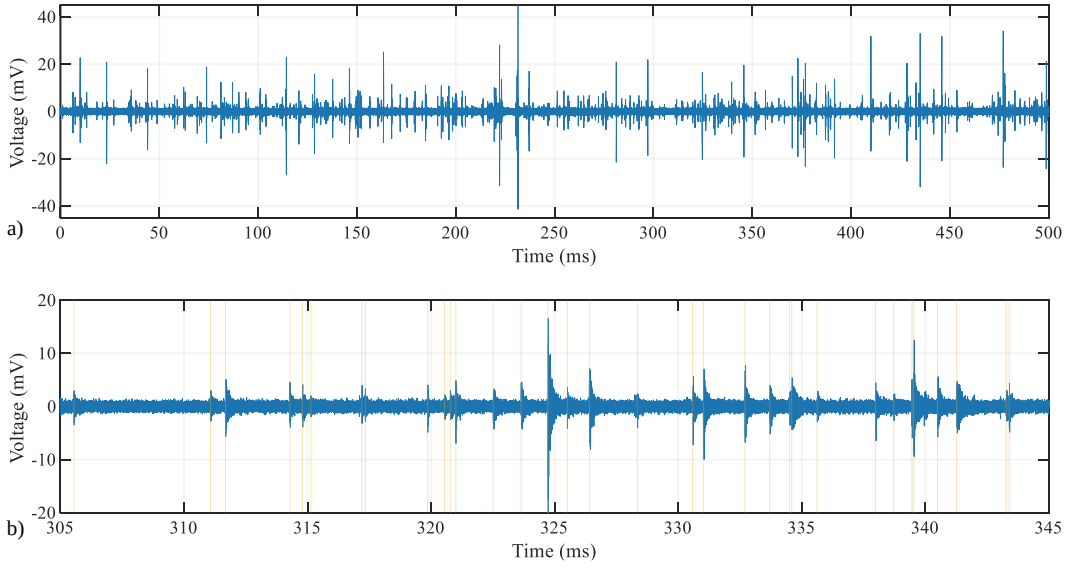

Fig. 10. (a) Signal frame used for the field data test-bench. (b) Zoom of 40ms of the signal frame, showing the ample variety on the incidence, lifespan and amplitudes of the AE waves present in the test-bench (manual onset picks indicated by the vertical yellow lines).

Following the methodology presented in [53], which is aimed to searching for acoustic waves in metallic components by means of the synchrosqueezed wavelet transform, for the case of the onset waves, the procedure for discriminating the presence of AE in the data-frame consisted of identifying the instant of time when the bi-dimensional manifold created by means of the energy contour mapping regarding to the original data-frame portrayed by the high-resolution SSWT became firstly closed by connecting all the modal frequencies of the signal of interest. Regarding to the endpoint determination, the detected AE events are considered finished when the energy corresponding regarding to the aforementioned manifold is vanished.

Fig. 11, depicts this procedure for five different AE events using a representative 1ms data-frame derived from the studied experiment showed in Fig. 10, which are located at 178.94-179.05, 179.25-179.27, 179.29-179.33, 179.34-179.38 and 179.40-179.49. In this instance it is show that by means of the high-resolution TFR, it is possible to easily discern between true AE events, and mechanical noises generated during the experiments and reflections generated due to energetic AE waves. Such is the case of the transient noises present at 179.2, 179.6 and 179.8ms, which in temporal domain could be associated with an AE source at the frequency domain they do not present any characteristic frequency content related to the AE phenomenon. Similarly, for reflections of events one and five located at 179.1 and 179.5ms respectively, it can be seen that despite of showing spectral content of representative AE frequencies, they are formed after the previous AE was vanished, thus, they can be discarded as true AE events.

Finally, for the case of the events two, three and four, which in the temporal domain could be easily discarded by presenting low energetic content, this particularly true for the fourth event by showing even less voltage amplitude than transient noise presented at 179.6ms; they energetic distributions in the TFR clearly show formant representative energies related to the AE phenomenon, thus, making possible to validate they nature as true AE events.

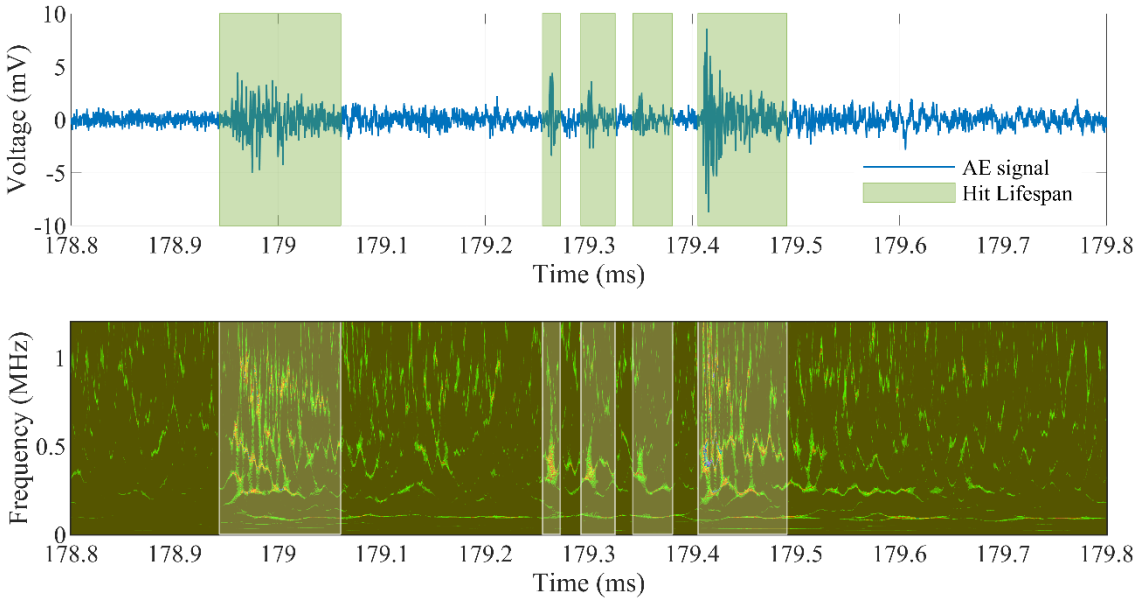

Fig. 11. Instance of 1ms containing five AE events derived from the tensile test, used to depicting the methodology for discarding the presence of AE events from noise and reflections. (a) Time-voltage representation. (b) High-resolution synchrosqueezing wavelet transform mapping.

4. Results and discussion

The competency of the STE-ZCR method is analyzed in front of two different experimental scenarios. Additionally, its performance is compared against four different representative AE detection techniques: (a) a classical threshold detector enhanced by means of the Instantaneous Amplitude envelope [24], (b) a STA/LTA detector [25], (c) a two-step Akaike Information Criterion picker [26], (d) and an Otsu detector working over a binary map image based on the Continuous Wavelet Transform [14], which as the AIC picker, it uses the same waveform derived from the Allen's Formula as characteristic function for the threshold-based early coarse detection.

4.1 Hsu-Nielsen data test-bench. Accuracy of the onset and endpoint determinations

As aforementioned, the objective for this test-bench is firstly to quantifying the accuracy of the measurement for the onset, endpoint and lifespans by means of the absolute error of each measure, and secondly to evaluate the operational robustness of detection in front of background noise.
For the calibration of the STE-ZCR method with regard to the corresponding temporal window analysis (type, length and overlapping factor), after a series of exhaustive trials, it was determined that one of the window functions that accomplished higher accuracy results was the Hamming implementation, in general those belonging to the raised cosine family. For the window overlapping factor, at expense of increasing the computational load, the best accuracy was achieved by maintaining the window overlapping to one sample, i.e., by directly convolving the instantaneous energy and the window function. Finally, the choice of the duration values of the window time, the threshold levels and the weighting factor for the noise analysis will be entirely determined by a prior calibration of the employed instrumentation as well as by the mechanical properties of the material. The calibration values of the comparative methods (see Table 1), was carried out following the recommendations of the related literature [26,42–46] as well as the current standards [8,9,47–51] of the AE discipline.

Table 1
Calibration parameters values used for each method for the Hsu-Nielsen test-bench.

Parameter	Method				
	IA	STA LTA	AIC	CWT Otsu	STE ZCR
Fixed threshold level	3e-3	5e-4	2e-1	2e-1	2e-4
Hit Definition Time [µs]	1e3		100	100	
Hit Lockout Time [µs]	10e3		10e3	10e3	
Threshold de-trigger		9e-5			
STA window time [µs]		75			
LTA window time [µs]		1e6			
Pre-event time [µs]		15			
Post-event time [µs]		10e3			
Weighting-R constant			4	4	
End delay time window 1 [µs]			25	25	
End delay time window 2 [µs]			10		
Start delay time window 1 [µs]				1.5e3	
Start delay time window 2 [µs]			100		
CWT scales				101	
Grayscale image bit-depth				16	
Median filter pixel neighbors				50	
STA length [µs]					20
STA window					Hamming
Overlapping window samples					1
ZCR threshold [%]					70
α-weighting STD noise					4
Early noise analysis [µs]					2e3

In Fig. 12 an instance of the manual onset pick procedure for an AE event is depicted. This is carried out by identifying the time instant when the bi-dimensional manifold created by means of the contour mapping of the SSWT becomes closed by connecting all the modal frequencies of the signal.

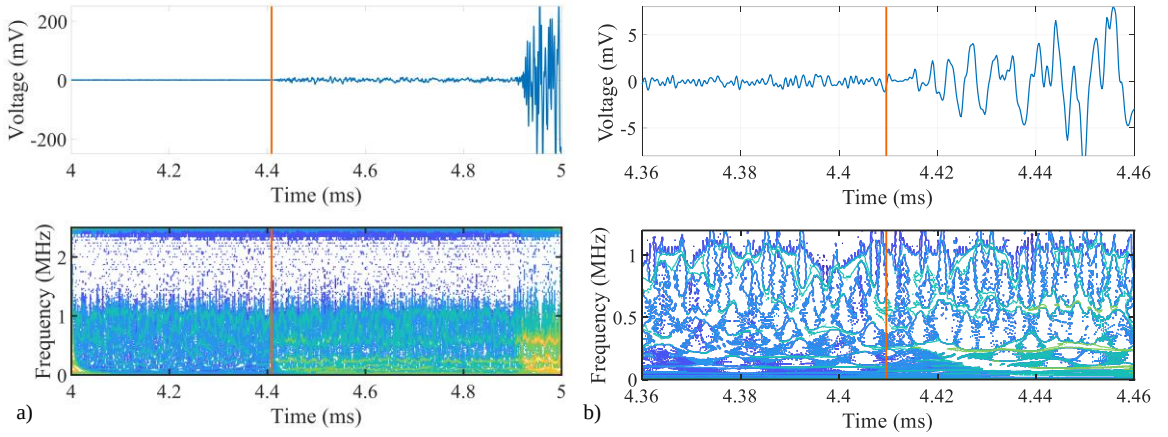

Fig. 12. Time-voltage and Time-Frequency representations corresponding to the onset of the synthetic AE wave showed in Fig. 6. (a) Data frame of 1ms displaying the onset location at 4.4084ms (vertical orange line) of the AE wave, and showing the energetic activity of the modal frequencies after the signal arrival in the TFR. (b) Zoom of 100μs of the data frame depicting the appearance in the TFR of the most energetic continuous ridge located at 263.12kHz, indicating the onset of the AE wave.

In Fig. 13 and Fig. 14, the resulting onset and endpoint automatic procedures for each method are depicted, using in all cases the same AE signal corresponding to Fig. 6.

For the onset determination, in Fig. 12 can be observed that due to the significant difference between the amplitudes of the primary wave (4.4 - 4.9ms) and the secondary wave (from 4.9ms on) regarding to the AE artificial source, all methods deal with a challenging signal in order to accurately determine the onset time. This condition forces to lower down the threshold level as minimum as possible for the IA and the STA/LTA methods at expense of increasing the chances to false-positive detections due to noise floor.

For the AIC and CWT-Otsu methods, since they perform an onset refinement detection procedure, they allow to maintain a higher threshold level for the early threshold detection with the aim to avoiding false-positive detections. Similarly, the STE-ZCR method through the onset refinement measure by means of the derivative of the STE, also allows to maintaining a higher threshold level in order to avoiding false-positive detections.

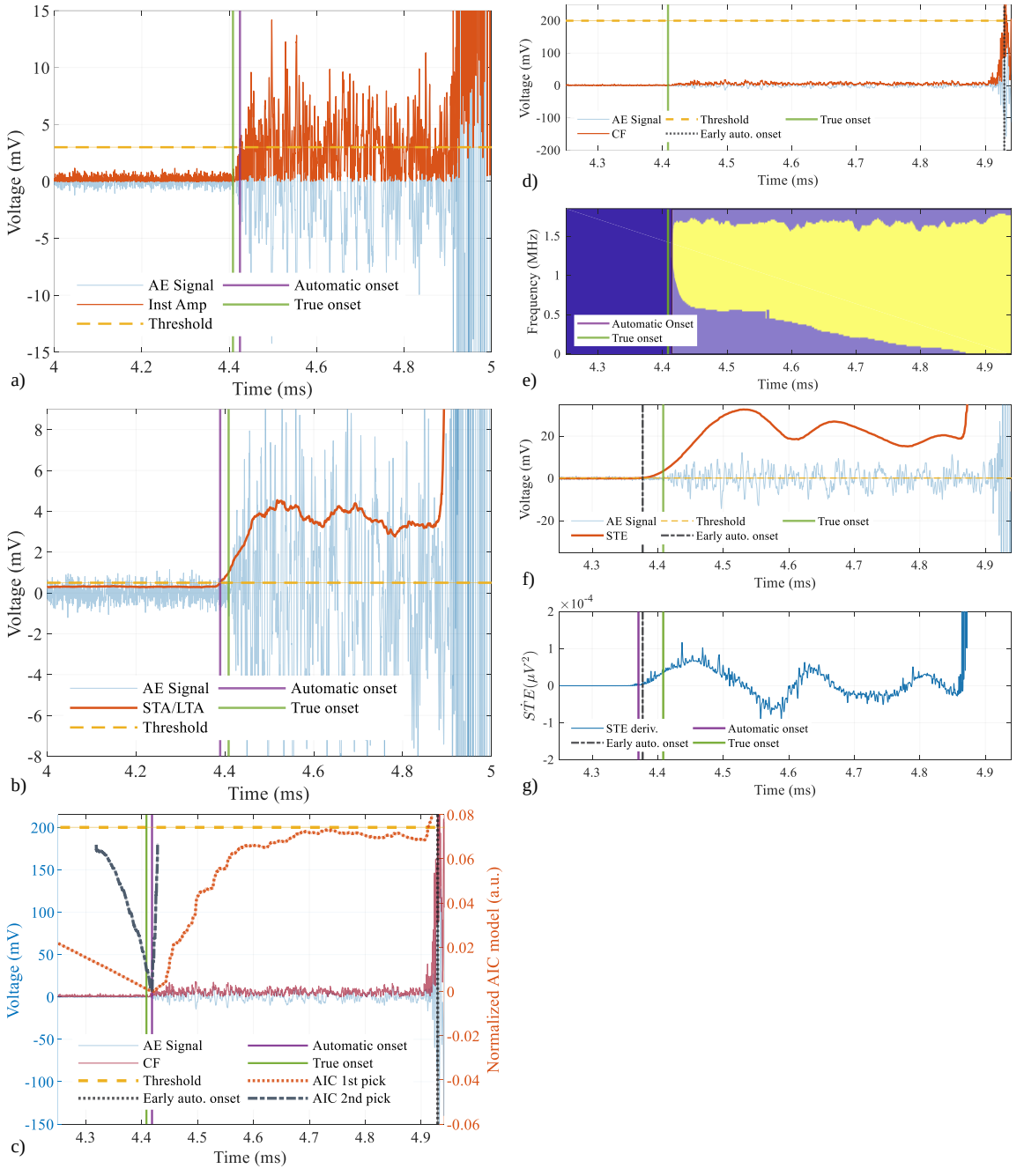

Fig. 13. Automatic onset detection procedure of the AE wave, corresponding to the methods: (a) Instantaneous amplitude, (b) STA/STL, (c) two-step AIC, (d) CWT-Otsu (early detection), (e) CWT-Otsu (detection refinement), (f) Short-Time Energy (early detection), (g) Short-Time Energy derivative (detection refinement). The onset absolute error corresponding to each method is calculated with regard to the manual True onset pick of the AE wave located at 4.4084ms for this instance (vertical green solid line), and the corresponding automatic onset pick (vertical lilac solid line) that each of the methods identifies.

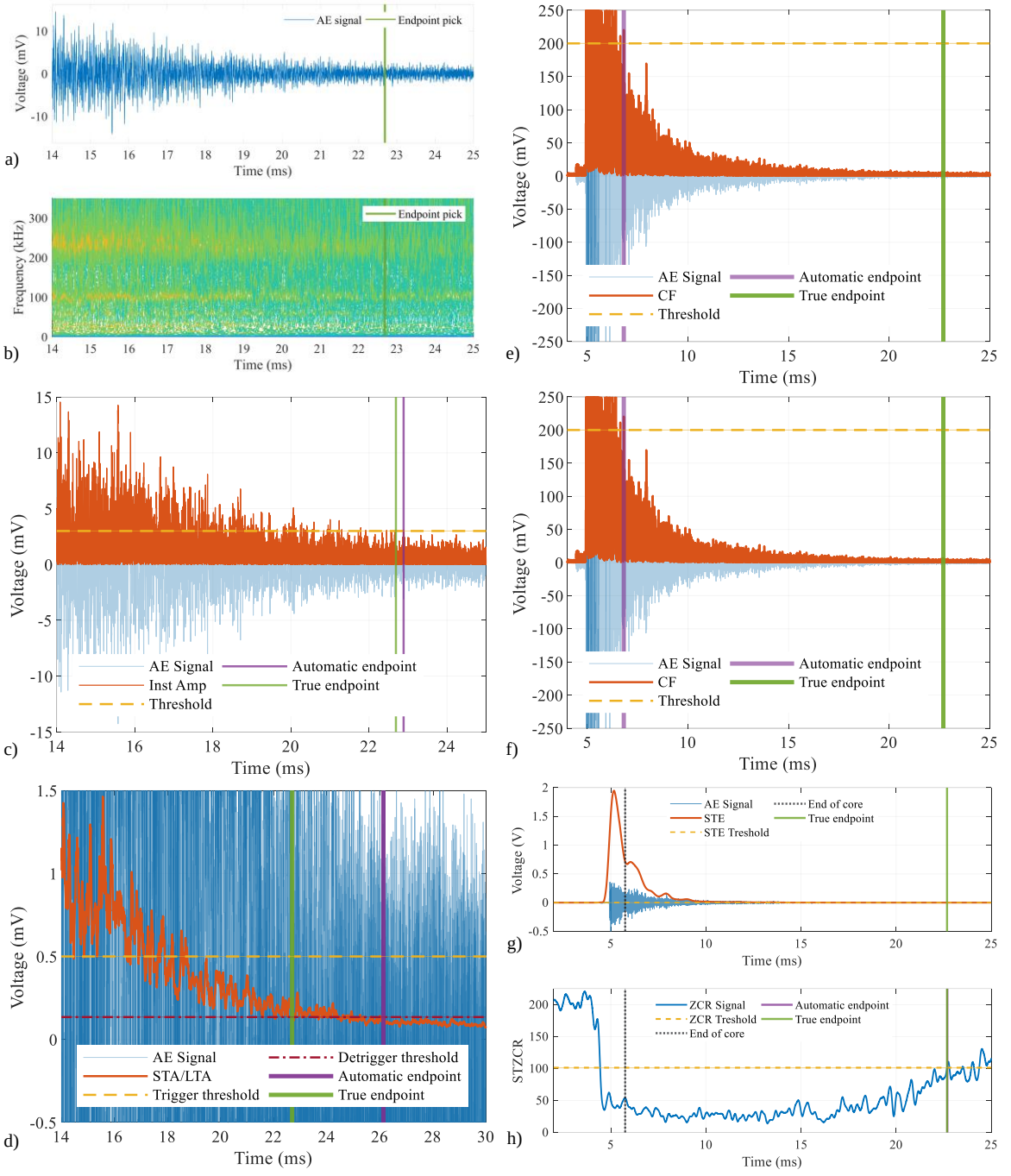

Fig. 14. Manual endpoint pick located at 22.6973ms for this instance (vertical green solid line), and identified when the bi-dimensional manifold created by means of the most energetic ridges of the SSWT is vanished, (a) Time-Voltage, (b) Time-Frequency. Automatic endpoint detection procedures of the AE wave corresponding to the methods: (c) Instantaneous amplitude, (d) STA/STL, (e) two-step AIC, (f) CWT-Otsu, (g) Short-Time Energy (early endpoint detection) and (g) Zero-Crossing Rate (detection refinement). The endpoint absolute error corresponding to each method is calculated with regard to the true endpoint of the AE wave.

For the endpoint detection case, in Fig. 14 (h) it is shown that by means the Zero-Crossing-Rate procedure although in order to be operative still makes use of a threshold value parameter, this characteristic function provides a reliable indicator in order to determine the conclusion of the signal. In contrast, Fig. 14 also shows that the other methods by making use of a combination of a threshold level along with preset fixed timer, preserve significant inaccuracies in the estimation of the end of the AE event.

In Table 2 it is shown the accuracy of the onset, endpoint and lifespan that each of the analyzed methods did quantified by means of the absolute error from the outcomes of the analyzed methods with regard to the manually picked instants of time. In Table 2, it is also showed the accuracy results for the operational robustness in front of three induced levels of background noise on the dataset. Finally, the average required consumed time in order to process an AE event belonging to the dataset is also displayed.

Table 2
Absolute error and standard deviation of the onset, endpoint and lifespan detections in regard with the Hsu-Nielsen test-bench.

Method	Onset error (μS)	Endpoint error (μs)	Lifespan error (μs)	Processing time (s)
IA (original signal)	-21.83 ± 8.26	2454 ± 1120	2476 ± 1120	2.53 ± 0.34
IA (SNR 20dB)	4271 ± 110.3	-20683 ± 1211	-24955 ± 1197	19.30 ± 2.32
IA (SNR 15dB)	4271 ± 110.4	-20504 ± 1273	-24776 ± 1263	22.94 ± 1.03
IA (SNR 10dB)	4271 ± 110.4	-20104 ± 1275	-24376 ± 1268	25.98 ± 1.59
STA/LTA (original signal)	-19.82 ± 7.92	3828 ± 1159	3848 ± 1161	1.56 ± 0.12
STA/LTA (SNR 20dB)	27.22 ± 185.44	3875 ± 1071	3848 ± 1161	1.58 ± 0.34
STA/LTA (SNR 15dB)	4256 ± 110.88	8104 ± 1174	3848 ± 1161	1.56 ± 0.11
STA/LTA (SNR 10dB)	4272 ± 110.39	8131 ± 1195	3902 ± 1197	1.60 ± 0.09
AIC (original signal)	-13.34 ± 7.00	16338 ± 1045	16352 ± 1045	2.98 ± 0.14
AIC (SNR 20dB)	-515.18 ± 7.31	18825 ± 1126	19340 ± 1126	3.09 ± 0.16
AIC (SNR 15dB)	-517.02 ± 6.96	18661 ± 1100	19178 ± 1100	3.24 ± 0.21
AIC (SNR 10dB)	2121 ± 2066	21959 ± 3108	19838 ± 1152	6.60 ± 9.92
CWT-Otsu (original signal)	-1.19 ± 97.88	17795 ± 1047	17796 ± 1039	1.57 ± 0.12
CWT-Otsu (SNR 20dB)	369.29 ± 582.2	18881 ± 1119	18447 ± 1301	1.67 ± 0.14
CWT-Otsu (SNR 15dB)	320.00 ± 647.9	18656 ± 1092	18336 ± 1309	1.85 ± 0.17
CWT-Otsu (SNR 10dB)	2425 ± 1892	21632 ± 3274	19207 ± 1763	4.52 ± 1.55
STE-ZCR (original signal)	3.29 ± 13.40	-0.63 ± 1797	3.31 ± 1800	0.013 ± 0.001
STE-ZCR (SNR 20dB)	-29.36 ± 12.13	9560 ± 2142	9589 ± 2145	0.029 ± 0.009
STE-ZCR (SNR 15dB)	-22.90 ± 193.7	11510 ± 4459	11533 ± 4467	0.027 ± 0.011
STE-ZCR (SNR 10dB)	236.5 ± 873.66	12986 ± 5788	12749 ± 5263	0.024 ± 0.009

For the onset detection measure, results indicate that all methods perform relatively well, accomplishing errors less than 20μs. However, the CWT-Otsu is the method that achieves the higher accuracy, obtaining an average error of only 1.19μs; still, at expense of displaying the largest dispersion error of the considered methods. For the STE-ZCR case, it reaches the second-best result, and also can be observed that the STE-ZCR method tends to detect the AE event before of its arrival, contrasting with the rest of the methods which are likely to determine the onset time after the actual start of the event.

For the endpoint detection case, results reveal that none of the comparative methods achieves a reliable measurement, yielding to absolute errors between two and four orders of magnitude with regard to the onset detection procedure. As observed in Fig. 14, this lack of accuracy owes that all methods make use of the

combination of threshold levels along with preset fixed timers (i.e., HDT, HLT, etc.), without considering the actual behavior of the signal. As consequence, these inaccuracies for the endpoint detection directly lead to errors to the lifespan determination. Contrarily, and despite of producing the result with higher dispersion and still depending on a calibration parameter, the STE-ZCR method achieves the best accuracy by considering an intrinsic indicator of the waveform.

For results regarding to the average consumed time to process each AE event, it can be observed that the most expensive technique corresponds to the two-step AIC, since it involves the refinement of the onset measure in two sequential instances, and having to modelling the signal in two occasions as consequence. For the IA technique, despite of performing the most basic approach of the considered methods, it achieved the second poorest performance on the test-bench, owing to that the searching-and-resetting scheme required to determine the endpoint time over a CF that exhibits a pronounced amount of rippling, is computationally expensive. The most balanced options are displayed by the STA/LTA and the CWT-Otsu methods, by reducing about to half of the required processing time with regarding to AIC and IA techniques. Still, for the case of the STE-ZCR method, since its operation is carried out on a very straightforward fashion, results show that its performance greatly excels to the current methods of the state of the art, achieving a reduction about of 99% of time regarding to the considered methods.

Finally, for the results corresponding to the operational robustness in front of induced AWG background noise, it was showed that the less resilient method corresponds to the IA technique, by saturating both measurements; i.e., by leading the onset detection to the start of the data frame and lagging the endpoint determination to the end of the data-frame at the first evaluation of added noise. Additionally, it also can be noticed that the required processing time did considerably increased when a greater amount of rippling was presented for its corresponding CF, due to higher levels of noise. For the STA/LTA method, by operating with a secondary threshold, which is aimed to determine the end of the AE event, their endpoint measurements showed some regularity during rounds of noise evaluations; additionally, the STA/LTA method proved to be the most resilient for the first evaluation of added noise due to the robustness delivered by its characteristic function, furthermore, the required processing time was sustained for all evaluations; however, by showing saturation the onset measurement failed for the 15 and 10dB ratios. The performance achieved by AIC technique in the onset determination, revealed some regularity for the 20 and 15dB ratios, nevertheless, this measurement failed for the 10dB ratio evaluation; for the endpoint measure case, by only depending on the threshold-timer scheme and by maintaining a high threshold level value for the test-bench, the obtained results were closed to those generated when the original signal was evaluated; however, they still showed considerable error amount; it also can be observed that while as the signal contained a greater presence of AWG noise the task of modelling the AE signal became more difficult for the AIC technique, and consequently impacting on the required processing time. Performance related to the onset determination achieved by the CWT-Otsu method, was the one that showed the closest coherence regarding to the AE phenomenon development, i.e., by properly detecting the arrival of the secondary waves for the 20 and 15dB ratios, nevertheless, accuracy was lost for the 10dB ratio; for the endpoint measure, by implementing the same scheme of the AIC in order to determine the conclusion of an AE event, results are equivalent to the aforementioned technique; for the analysis of the average consumed time per AE event, the technique showed a tolerable time consumption when analyzing three levels of induced AWGN relating to the original signal obtained results. For the case of the STE-ZCR method, due to implementing a threshold adjustment procedure based on the early estimation of noise floor, the technique proved to be the most resilient alternative for the onset detection measure in comparison with the considered methods, by considerably reducing the amount of error as well as never saturating the detections; for the endpoint determination and despite of having been heavily biased by the induced AWGN, the measured based on the ZCR characteristic function showed coherence as regards to the AE phenomenon development; finally, concerning to the required average processing time, the STE-ZCR method proved to be

the most efficient alternative by practically maintaining unaltered the performance metrics obtained by analyzing the original signal.

4.2 Uniaxial tensile test. Quality of detection statistical indicators

Objective for this second test-bench is to quantify the quality of event detection over a data frame collected from a standardized tensile test, which contains a substantial diversity of continuous AE events. Contrasting to the artificial AE events produced by the Hsu-Nielsen procedure, real AE waves typically will exhibit smaller amplitudes and shorter durations, of course depending on the stage of damage of the specimen under evaluation. Therefore, for the calibration used for this test-bench (see Table 3), the time-driven parameters as well as the threshold levels have been reduced in order to increase the sensitivity of the considered techniques, regarding to temporal and amplitude detection capabilities.

Table 3
Calibration parameters values used for each method for the field data test-bench.

Parameter	Method				
	IA	STA LTA	AIC	CWT Otsu	STE ZCR
Fixed threshold level	2.25e-3	4e-3	6e-3	6e-3	55e-6
Hit Definition Time [μs]	100		100	100	
Hit Lockout Time [μs]	15		15	15	
Threshold de-trigger		3e-3			
STA window time [μs]		25			
LTA window time [μs]		10e3			
Pre-event time [μs]		1			
Post-event time [μs]		0.5			
Weighting-R constant			4	4	
End delay time window 1 [μs]			10	10	
End delay time window 2 [μs]			5		
Start delay time window 1 [μs]				75	
Start delay time window 2 [μs]			20		
CWT scales				101	
Grayscale image bit-depth				16	
Median filter pixel neighbors				50	
STA duration [μs]					15
STA window					Hamming
Overlapping window samples					1
ZCR threshold [%]					80
α-weighting STD noise					1
Early noise analysis [μs]					5

Once that all methods have processed the field data frame of 500ms length, the quality of event detection is quantified in two steps. Firstly, by counting the total number of detected events against the true temporal locations referring to the total amount of 380 AE events present in the data frame. And secondly, by classifying the properly detected events (true-positive), missed events (false-negative) and the mistakenly detected events (false-positive), that each method concludes (see Table 4).

Table 4
Classification of the identified events regarding to 380 AE waves present in the data frame.

	Method				
	IA	STA/LTA	AIC	CWT-Otsu	STE-ZCR
Total detections	373	380	372	372	367
True-positive	322	324	299	299	338
False-negative	58	56	81	81	42
False-positive	51	56	73	73	29

For this field data test-bench, and from the total number of true-positive detected events, the absolute error for the onset, endpoint and lifespan are also calculated (see Table 5).

Table 5
Absolute error and standard deviation of the onset, endpoint and lifespan detections regarding to the field data test-bench.

Method	Onset error (μs)	Endpoint error (μs)	Lifespan error (μs)
IA	-9.69 ± 7.56	38.39 ± 101.27	48.09 ± 102.13
STA/LTA	-2.49 ± 8.63	12.07 ± 83.65	14.56 ± 84.85
AIC	-6.15 ± 10.44	19.57 ± 543.74	50.4 ± 692.6
CWT-Otsu	2.53 ± 29.45	-92.36 ± 97.4	89.82 ± 97.74
STE-ZCR	4.62 ± 53.79	-4.42 ± 114.15	-9.05 ± 102.04

From Table 5, it can be observed that in comparison with the Hsu-Nielsen test-bench, error is reduced and better aligned with the results obtained for the first round of operative robustness (SNR 20dB); this, due to having to deal with less challenging AE events by showing less pronounced s-waves. For the onset detection, all methods performed with sustained accuracy by achieving an average error lesser than 10μs in all cases.

In this experimental scenario, the STE-ZCR method also accomplished the best endpoint determinations and in consequence the best lifespan measures, assuring that most of the detected events are completely detected, this particularly critical in case of subsequent assessing analysis.

From results of Table 4, it also can be observed that despite that in average, all methods nearly detect 99% of the detection objective, i.e., 380-hits; none of them reaches more than 85% of true-positive detections. In consequence, given the quality with which these detections are performed, the reliability of the methods is not guaranteed. In Fig. 15, it is shown the detection outcomes of all considered methods, using the representative five AE events afore showed in Fig. 11.

As it can be observed in Fig. 15, none of the analyzed methods achieves the required detections without errors. Such is the case of the Instantaneous Amplitude method, which after the first event detection it splices four AE events as if it was a single one, this error owes to the use of the threshold level along with the fixed Hit Definition Timer for the endpoint detection corresponding to the second event. For the STA/LTA method, its characteristic function helps to depicting with higher accuracy the dynamic of the AE phenomenon and therefore to detecting more events; nevertheless, by implementing the same procedure of a threshold level and a fixed timer, it splices the second and third event as a single detection; finally, the STA/LTA method also executes a false-positive detection corresponding to the reflection of the last AE wave.

In this instance, it is also clear that AIC and CWT-Otsu methods mandatorily require a precise early onset estimation with the aim to achieving a consistent onset automatic refinement, since after properly detecting the first AE event, the less energetic events are discarded, i.e., the second, third and fourth events; this by detecting the fifth AE event as the start of the wave, and in consequence leading to three false-negative detections. Finally, the STE-ZCR method despite of also executing the same false-positive detection as the STA/LTA technique (located at 179.6ms), it can be observed that besides of achieving the most accurate lifespan measures, it is the only method that accomplishes the detection of all existing AE events.

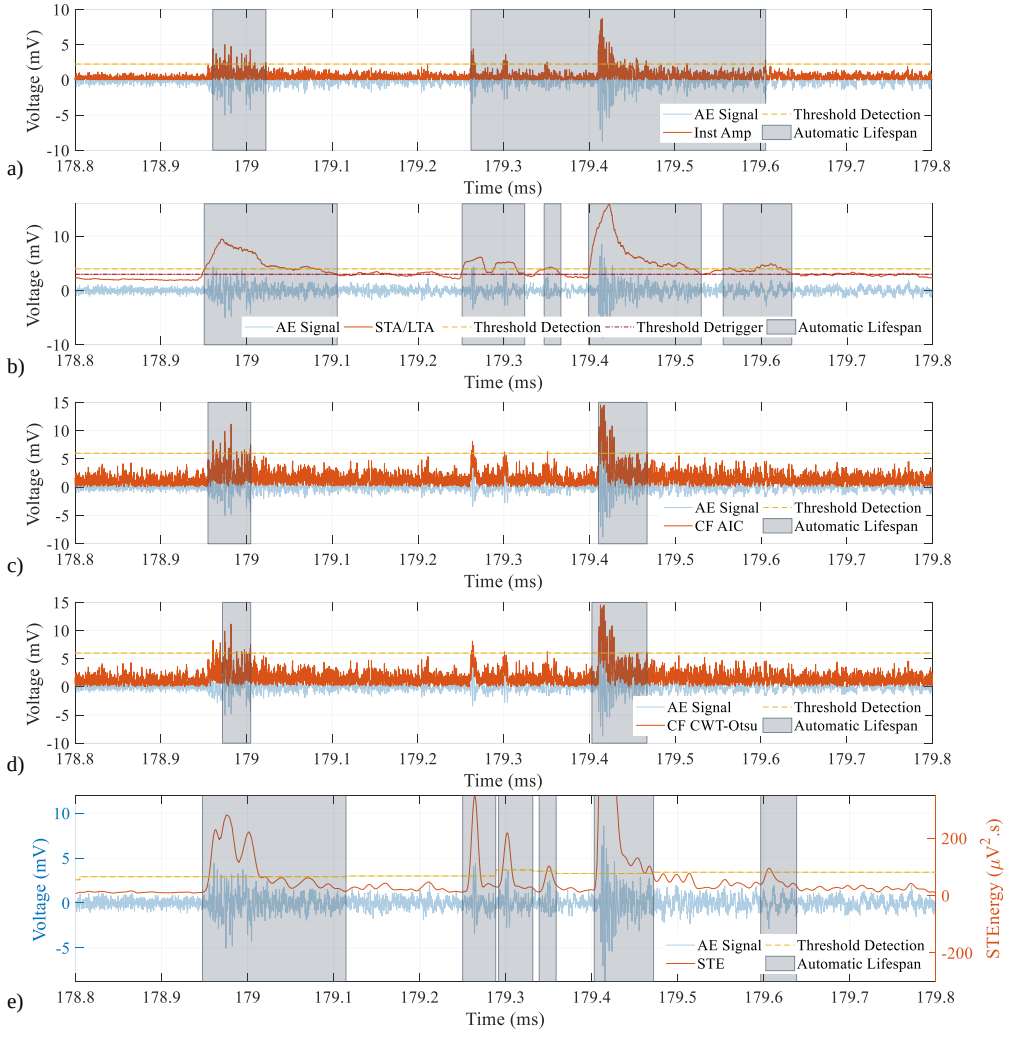

Fig. 15. Comparison of AE events automatically detected by the considered methods for an instance of 1ms (derived from the uniaxial tensile test). (a) Instantaneous Amplitude, (b) STA/LTA, (c) AIC, (d) CWT-Otsu and (d) STE-ZCR proposed technique.

Finally, in this test-bench is quantified the quality of event detection of the considered methods. For this, by means of the number of classified AE events from Table 4, a set of statistical indicators are calculated.

These are: (a) accuracy (the ratio of true-positive events to all detected and not detected events), (b) precision (the ratio of true-positive events to the amount of true and false-positive events), (c) sensitivity (the ratio of true positive events to the sum of true-positive and false-negative detections), (d) F1-score (the harmonic average between precision and sensitivity), (e) false discovery rate (the ratio of false-positive detections to all detected events), (f) false-negative rate (the ratio of false-negative detections to the sum of false-negative and true-positive events), see Table 6.

Table 6
Statistical metrics corresponding to the quality for event detection concerning to the data field test-bench.

	Method				
	IA	STA/LTA	AIC	CWT Otsu	STE ZCR
Accuracy (%)	74.71	74.31	66.00	66.00	82.64
Precision (%)	86.33	85.26	80.38	80.38	92.10
Sensitivity (%)	84.74	85.26	78.68	78.68	88.95
F1 score (%)	85.52	85.26	79.52	79.52	90.50
False discovery rate (%)	13.67	14.74	19.62	19.62	7.90
False negative rate (%)	15.26	14.74	21.32	21.32	11.05
Processing time (sec.)	220.49	33.54	608.56	182.92	19.6

For this test-bench, Table 6 shows that the comparative methods perform with reasonable confidence by achieving an average accuracy of 70% of the required detections, also can be noticed that this accuracy score is consistently aligned with the endpoint determination. In general terms, all methods achieved better results in the precision score than in the accuracy score, this due to the presence in the dataset of larger true AE events with regard to false events in form of high-energy reflections and mechanical noises. For the sensitivity score, all methods slightly diminished their performances regarding to the precision metric, this, due to slightly being prone to generating false-negative detections, mostly of them derived from spliced detections.

For the case of the STE-ZCR method, it exceled to the rest of the considered techniques about 12% for the accuracy metric, 10% for the precision metric, 7% for the sensitivity metric, 8% for the F1-score, 10% for the false discovery rate and 7% for the false negative rate. This improvement clearly owes to performing the endpoint determination with higher accuracy. Finally, it can also be observed that in comparison with the considered methods, the STE-ZCR technique reduces the required processing time about 45-97% in order to process the data frame.

5. Conclusions

An Acoustic Emission activity detector, which allows an automatic and continuous detection of AE events, was developed using time domain features obtained from the waveform of the signal of interest. The proposed methodology was realized by revisiting a well-established signal processing technique from the speech processing area, and adapting it to the requirements of the AE phenomenon.

Two experimental scenarios were arranged with the aim to quantifying the performance of the proposed method, and with the aim to analyzing three critical aspects related to the AE event detection: the onset and endpoint accuracies, as well the quality for detecting said events.

Firstly, for the experimental scenario using artificial Hsu-Nielsen sources, in the case of the onset detection measure, the proposed STE-ZCR method improved the accuracy with regard to the IA method by diminishing the error of the measures by 85%, 83% for the STA/LTA and 75% for the AIC method. For the case of the CWT-Otsu technique, and despite of producing larger average error, the STE-ZCR method improved the respective dispersion error by 86%.
For the endpoint detection measure, by implementing an indicator derived from the waveform of the AE signal, the STE-ZCR method surpassed the accuracy of the comparative techniques in about four and five orders of magnitude, which also contributed to achieving the lowest error for the lifespan measure.

Lastly in this Hsu-Nielsen test, due to implementing an adaptive threshold scheme, the STE-ZCR proved to be the most resilient method under noisy scenarios by never saturated the measurements.

Secondly, for the field-data derived from the uniaxial test, besides of having verified that the obtained results for the onset and endpoint measures of the considered methods are consistent with the obtained for the Hsu-Nielsen test, it was studied the quality with which the AE events are detected.
Results showed that for a data-frame of 500ms, containing 380 AE events of different durations, amplitudes and manifesting randomly, the STE-ZCR was the method that achieved the highest amount of true-positive detections and the lowest amount of false identifications, both positive and negative. Quantitatively the STE-ZCR method excelled to the rest of the considered techniques in average about 12% for the accuracy, 10% for the precision and 7% for the sensitivity; while simultaneously reduced in average around of 10% and 7% the false discovery and the false negative rate cases respectively. Once again, this improvement responds to the fact of implementing a dedicated indicator with aim to detecting the end of the AE events.

Furthermore, by implementing a straightforward processing scheme, the proposed STE-ZCR method was the one that achieved the best processing times for both experimental scenarios, by reducing the required search times from one up to three orders of magnitude regarding to the compared techniques.

It must be noted that despite that the STE-ZCR AE activity detector was developed for applications related to the characterization of metallic components, by only requiring the waveform of the AE phenomenon to operate, its use for another AE applications and materials could be feasible.

Finally, its straightforward scheme and the diminished consumption times, suggests a possible and efficient hardware implementation for online monitoring applications. Moreover, with the aim of reducing the payload required to transmit or store the large data streams demanded by the AE phenomenon, by achieving an adequate identification and separation of the events, it could be possible to subsequently only working with the detected events instead of the entire data stream.

Acknowledgments

This work was partially supported by the CONACyT (Consejo Nacional de Ciencia y Tecnología, México) with the scholarship 411711; and by the Spanish Ministry of Economy and Competitiveness, under the TRA2016-80472-R Research Project.

References

[1] J. Hirsch, T. Al-Samman, Superior light metals by texture engineering: Optimized aluminum and magnesium alloys for automotive applications, Acta Mater. 61 (2013) 818–843. doi:10.1016/j.actamat.2012.10.044.

[2] M.K. Kulekci, Magnesium and its alloys applications in automotive industry, Int. J. Adv. Manuf. Technol. 39 (2008) 851–865. doi:10.1007/s00170-007-1279-2.

[3] ASTM Standard E8/E8M, 2016 (1991), Standard Test Methods for Tension Testing of Metallic Materials, Am. Soc. Test. Mater. (2016) 1–27. doi:10.1520/E0008_E0008M-16A.

[4] ISO Standard 6892-1:2016, Metallic materials - Tensile testing - Part 1: Method of test at room temperature, International Organization for Standardization, Geneva, Switzerland, 2016. doi:10.3403/30268532.

[5] L. Tian, L. Yu, B. Pan, Accuracy enhancement of a video extensometer by real-time error compensation, Opt. Lasers Eng. 110 (2018) 272–278. doi:10.1016/j.optlaseng.2018.06.010.

[6] E. Martinez-Gonzalez, I. Picas, D. Casellas, J. Romeu, Detection of crack nucleation and growth in tool steels using fracture

tests and acoustic emission, Meccanica. 50 (2015) 1155–1166. doi:10.1007/s11012-013-9858-9.

[7] C.J. Hellier, Acoustic Emission Testing, in: Handb. Nondestruct. Eval., Second Edi, McGraw-Hill Education, New York, 2013. doi:10.1036/007177713X.ch10.

[8] ASTM International, ASTM E750-15, Standard Practice for Characterizing Acoustic Emission Instrumentation, ASTM International, West Conshohocken, PA, 2015. doi:10.1520/E0750-15.

[9] I.O. for Standardization, ISO 12716:2001, Non-destructive testing -- Acoustic emission inspection, 2017.

[10] D. Bianchi, E. Mayrhofer, M. Gröschl, G. Betz, A. Vernes, Wavelet packet transform for detection of single events in acoustic emission signals, Mech. Syst. Signal Process. 64–65 (2015) 441–451. doi:10.1016/j.ymssp.2015.04.014.

[11] A. Gupta, J.C. Duke, Identifying the arrival of extensional and flexural wave modes using wavelet decomposition of ultrasonic signals, Ultrasonics. 82 (2018) 261–271. doi:10.1016/j.ultras.2017.09.008.

[12] E. Pomponi, A. Vinogradov, A. Danyuk, Wavelet based approach to signal activity detection and phase picking: Application to acoustic emission, Signal Processing. 115 (2015) 110–119. doi:10.1016/j.sigpro.2015.03.016.

[13] A. Danyuk, I. Rastegaev, E. Pomponi, M. Linderov, D. Merson, Improving of acoustic emission signal detection for fatigue fracture monitoring, Procedia Eng. 176 (2017) 284–290. doi:10.1016/j.proeng.2017.02.323.

[14] F. Bai, D. Gagar, P. Foote, Y. Zhao, Comparison of alternatives to amplitude thresholding for onset detection of acoustic emission signals, Mech. Syst. Signal Process. 84 (2017) 717–730. doi:10.1016/j.ymssp.2016.09.004.

[15] R. V. Allen, Automatic earthquake recognition and timing from single traces, Bull. Seismol. Soc. Am. 68 (1978) 1521–1532. http://www.bssaonline.org/content/68/5/1521.short.

[16] J.H. Kurz, C.U. Grosse, H.-W. Reinhardt, Strategies for reliable automatic onset time picking of acoustic emissions and of ultrasound signals in concrete, Ultrasonics. 43 (2005) 538–546. doi:10.1016/j.ultras.2004.12.005.

[17] F. Piñal Moctezuma, M. Delgado Prieto, L. Romeral Martinez, Performance Analysis of Acoustic Emission Hit Detection Methods Using Time Features, IEEE Access. 7 (2019) 71119–71130. doi:10.1109/ACCESS.2019.2919224.

[18] M. Kang, J. Kim, J.-M. Kim, An FPGA-Based Multicore System for Real-Time Bearing Fault Diagnosis Using Ultrasampling Rate AE Signals, IEEE Trans. Ind. Electron. 62 (2015) 2319–2329. doi:10.1109/TIE.2014.2361317.

[19] S. Wirtz, A. Cunha, M. Labusch, G. Marzun, S. Barcikowski, D. Söffker, Development of A Low-Cost FPGA-Based Measurement System for Real-Time Processing of Acoustic Emission Data: Proof of Concept Using Control of Pulsed Laser Ablation in Liquids, Sensors. 18 (2018) 1775. doi:10.3390/s18061775.

[20] Y. Hu, L. Wang, X. Huang, X. Qian, L. Gao, Y. Yan, On-line sizing of pneumatically conveyed particles through acoustic emission detection and signal analysis, IEEE Trans. Instrum. Meas. 64 (2015) 1100–1109. doi:10.1109/TIM.2014.2355653.

[21] A. Sehgal, N. Kehtarnavaz, A Convolutional Neural Network Smartphone App for Real-Time Voice Activity Detection, IEEE Access. 6 (2018) 9017–9026. doi:10.1109/ACCESS.2018.2800728.

[22] European Telecommunications Standards Institute, TS 126 194. Digital cellular telecommunications system (Phase 2+) (GSM); Universal Mobile Telecommunications System (UMTS); LTE; Speech codec speech processing functions; Adaptive Multi-Rate - Wideband (AMR-WB) speech codec; Voice Activity Detector (VAD)., 2018. https://www.etsi.org.

[23] L.R. Rabiner, M.R. Sambur, An Algorithm for Determining the Endpoints of Isolated Utterances, Bell Syst. Tech. J. 54 (1975) 297–315. doi:10.1002/j.1538-7305.1975.tb02840.x.

[24] E. Dehghan Niri, A. Farhidzadeh, S. Salamone, Nonlinear Kalman Filtering for acoustic emission source localization in anisotropic panels, Ultrasonics. 54 (2014) 486–501. doi:10.1016/j.ultras.2013.07.016.

[25] P. Bormann, Understanding and parameter setting of STA/LTA trigger algorithm, Bormann, P.(Ur.). 1 (2011) 1–34. doi:10.2312/GFZ.NMSOP-2_IS_8.1.

[26] P. Sedlak, Y. Hirose, M. Enoki, Acoustic emission localization in thin multi-layer plates using first-arrival determination, Mech. Syst. Signal Process. 36 (2013) 636–649. doi:10.1016/j.ymssp.2012.11.008.

[27] N.N. Kulkarni, V.K. Bairagi, Extracting Salient Features for EEG-based Diagnosis of Alzheimer's Disease Using Support Vector Machine Classifier, IETE J. Res. 63 (2017) 11–22. doi:10.1080/03772063.2016.1241164.

[28] T. Giannakopoulos, A. Pikrakis, Introduction to Audio Analysis: A MATLAB Approach, 2014. doi:10.1016/C2012-0-03524-

7.

[29] D. Mitrović, M. Zeppelzauer, C. Breiteneder, Features for Content-Based Audio Retrieval, in: Introd. to Audio Anal., Elsevier, 2010: pp. 71–150. doi:10.1016/S0065-2458(10)78003-7.

[30] J. Griffin, Traceability of Acoustic Emission measurements for a proposed calibration method - Classification of characteristics and identification using signal analysis, Mech. Syst. Signal Process. 50–51 (2015) 757–783. doi:10.1016/j.ymssp.2014.04.018.

[31] D. Sánchez-Molina, E. Martínez-González, J. Velázquez-Ameijide, J. Llumà, M.C.R. Soria, C. Arregui-Dalmases, A stochastic model for soft tissue failure using acoustic emission data, J. Mech. Behav. Biomed. Mater. 51 (2015) 328–336. doi:10.1016/j.jmbbm.2015.07.002.

[32] Z. Nazarchuk, V. Skalskyi, O. Serhiyenko, Handbook of Technical Diagnostics, Springer Berlin Heidelberg, Berlin, Heidelberg, 2013. doi:10.1007/978-3-642-25850-3.

[33] R.W.B. Stephens, A.A. Pollock, Waveforms and Frequency Spectra of Acoustic Emissions, J. Acoust. Soc. Am. 50 (1971) 904–910. doi:10.1121/1.1912715.

[34] L. Bolin, A model for estimating the signal from an acoustic emission source, Ultrasonics. 17 (1979) 67–70. doi:10.1016/0041-624X(79)90098-2.

[35] C. D'Attellis, L. Pérez, D. Rubio, J. Ruzzante, A Bank of Kalman Filters for Failure Detection Using Acoustic Emission Signals, in: Non-Destructive Test. '92, Elsevier, 1992: pp. 29–33. doi:10.1016/B978-0-444-89791-6.50012-3.

[36] K. Nadolny, P. Sutowski, D. Herman, Analysis of aluminum oxynitride AlON (Abral®) abrasive grains during the brittle fracture process using stress-wave emission techniques, Int. J. Adv. Manuf. Technol. 81 (2015) 1961–1976. doi:10.1007/s00170-015-7338-1.

[37] M.I. López Pumarega, Relation between Amplitude and Duration of Acoustic Emission Signals, in: AIP Conf. Proc., AIP, 2003: pp. 1431–1438. doi:10.1063/1.1570299.

[38] N. Casiez, S. Deschanel, T. Monnier, O. Lame, Acoustic emission from the initiation of plastic deformation of Polyethylenes during tensile tests, Polymer (Guildf). 55 (2014) 6561–6568. doi:10.1016/j.polymer.2014.09.044.

[39] D. Wotzka, Mathematical Model and Regression Analysis of Acoustic Emission Signals Generated by Partial Discharges, Appl. Comput. Math. 3 (2014) 225. doi:10.11648/j.acm.20140305.15.

[40] D. Wotzka, T. Boczar, P. Fracz, Mathematical Model and Numerical Analysis of AE Wave Generated by Partial Discharges, Acta Phys. Pol. A. 120 (2011) 767–771. doi:10.12693/APhysPolA.120.767.

[41] I. Daubechies, J. Lu, H.-T. Wu, Synchrosqueezed wavelet transforms: An empirical mode decomposition-like tool, Appl. Comput. Harmon. Anal. 30 (2011) 243–261. doi:10.1016/j.acha.2010.08.002.

[42] K. Ono, Calibration Methods of Acoustic Emission Sensors, Materials (Basel). 9 (2016) 508. doi:10.3390/ma9070508.

[43] N. Md Nor, A. Ibrahim, N. Muhamad Bunnori, H.M. Saman, S.N. Mat Saliah, S. Shahidan, Diagnostic of fatigue damage severity on reinforced concrete beam using acoustic emission technique, Eng. Fail. Anal. 41 (2014) 1–9. doi:10.1016/j.engfailanal.2013.07.015.

[44] G.C. McLaskey, D.A. Lockner, Calibrated Acoustic Emission System Records M −3.5 to M −8 Events Generated on a Saw-Cut Granite Sample, Rock Mech. Rock Eng. 49 (2016) 4527–4536. doi:10.1007/s00603-016-1082-1.

[45] D. Fettré, J. Favergeon, S. Bouvier, Detection of Breakaway for a High-Temperature Oxidation of Pure Zirconium Using Acoustic Emission Correlated to Thermogravimetry, Oxid. Met. 87 (2017) 367–379. doi:10.1007/s11085-017-9737-1.

[46] E. Dehghan-Niri, A. Farhidzadeh, S. Salamone, Determination of the probability zone for acoustic emission source location in cylindrical shell structures, Mech. Syst. Signal Process. 60–61 (2015) 971–985. doi:https://doi.org/10.1016/j.ymssp.2015.02.004.

[47] ASTM International, ASTM E976-15, Standard Guide for Determining the Reproducibility of Acoustic Emission Sensor Response, 2015. doi:10.1520/E0976-15.

[48] ASTM International, ASTM E650 / E650M-17, Standard Guide for Mounting Piezoelectric Acoustic Emission Sensors, 2017. doi:10.1520/E0650_E0650M-17.

[49] ASTM International, ASTM E2374-16, Standard Guide for Acoustic Emission System Performance Verification, 2016.

doi:10.1520/E2374-16.

[50] ASTM International, ASTM E1932-12(2017), Standard Guide for Acoustic Emission Examination of Small Parts, 2017. doi:10.1520/E1932-12R17.

[51] ASTM International, ASTM E1106-12(2017), Standard Test Method for Primary Calibration of Acoustic Emission Sensors, 2017. doi:10.1520/E1106-12R17.

[52] U. of S.C. LAMSS, Wavescope: Dispersion curves, group velocities, and tuning for metallic structures, (2010). http://www.me.sc.edu/Research/lamss/NV/html/L_software.html.

[53] H. Selim, F. Piñal Moctezuma, M. Delgado Prieto, J. Francisco Trull, L. Romeral Martínez, C. Cojocaru, Wavelet Transform Applied to Internal Defect Detection by Means of Laser Ultrasound, in: Wavelet Transform Complex. [Working Title], IntechOpen, 2019: p. 13. doi:10.5772/intechopen.84964.